Array Beampattern Synthesis Without Specifying Lobe Level Masks

Junli Liang, Xuhui Fan, Hing Cheung So, *Fellow, IEEE*, and Deyun Zhou

***Abstract*— In this article, we devise a novel array beampattern synthesis algorithm, namely, without lobe level mask (WLLM), to avoid specifying a possibly improper or infeasible pattern mask by minimizing the ratio of the maximal sidelobe level to the minimal mainlobe level. To solve the resultant nonconvex and nonlinear fractional programming, we introduce auxiliary exponent variables to separate the numerator and denominator, and simplify each of the corresponding subproblems as a special single-variable optimization problem with a piecewise objective function and the constraints are removed via introducing unit-step functions. We also analyze the convexity or concavity of each piecewise function to compute the corresponding local minimum from which the global minimum can be obtained. Furthermore, our developed method is extended for solving the phase-only and constant modulus pattern synthesis problems. Numerical examples show that the WLLM beampattern synthesis methods can attain sufficiently low sidelobe level relative to the mainlobe level and is suitable for arbitrary array configurations.**

***Index Terms*— Beampattern synthesis, fractional programming, nonconvex and nonlinear optimization, without lobe level mask (WLLM).**

I. Introduction

THE task of beampattern synthesis is to find a weight vector for an antenna array in order to produce a specified radiation pattern [1]–[15]. It is widely applied in different fields of array signal processing, including microphone arrays, radar, and sonar and thus has received a significant amount of attention.

In general, there are two ideas to specify the pattern masks in a robust manner for practical scenarios [1]–[15]. One is to set the mainlobe level and response ripple by considering the need that the provided direction-of-arrival of signal-of-interest is usually imprecise [1], [2], [15]. Another is to specify the sidelobe level by noting that there is no prior information about the approximate locations of strong interferences [1], [2], [15]. When one of the following cases happens: 1) the specified sidelobe level (mainlobe level) is too small (large) and 2) the mainlobe ripple term is too small, the specified mask for the pattern synthesis task is possibly improper or infeasible to achieve, especially for phase-only [16]–[21] and constant modulus pattern synthesis problems [21], [22] resulted from the fact that there are finite degrees-of-freedom for the weight vector. Obviously, it is necessary to avoid specifying a possibly improper or mathematical infeasible mask for pattern synthesis problems, especially for the phase-only and constant modulus pattern synthesis problems.

Unlike the standard synthesis methods [1]–[22], this article focuses on the beampattern synthesis problem without specifying lobe level masks. On the one hand, we may avoid specifying a possibly improper or infeasible pattern mask. On the other hand, we can attain the minimal ratio of the sidelobe level to the mainlobe level, which implies sufficiently low sidelobe level with respect to the mainlobe level and thus is helpful to improve the electronic countermeasure capability. In this article, we present two beampattern synthesis methods without specifying lobe level masks, referred as without lobe level mask (WLLM). Note that we have recently developed solutions to the phase-only [21] and sparse array [23] beampattern synthesis problems, where the lobe level masks are specified. Our contributions to this article are highlighted as follows.

1) To avoid specifying a possibly improper or infeasible pattern mask, we formulate a fractional program for array beampattern synthesis. Especially, the denominator and numerator are the smallest mainlobe level and largest sidelobe level, respectively. Therefore, in some sense, the proposed metric is robust against the worst case, where the interference appears at the angle with the maximal sidelobe level and the target appears at the angle with the minimal mainlobe level.
2) To solve such a difficult nonconvex and nonlinear optimization problem, we introduce auxiliary exponent variables to separate the numerator and denominator and thus divide the fractional optimization problem into two independent subproblems.
3) We simplify each subproblem as a special single-variable optimization problem with a piecewise objective function and with no constraints via exploiting unit-step functions. Then the convexity or concavity of each piecewise function is analyzed to compute the local minima from which the global solution can be obtained.
4) For the phase-only [16]–[21] and constant modulus [21]–[22] pattern synthesis problems without lobe level masks, we derive the corresponding equivalent problems with unknown modulus. In particular, we simplify the complex variable vector update problem into a special

Manuscript received May 6, 2018; revised October 15, 2019; accepted January 24, 2020. Date of publication February 13, 2020; date of current version June 2, 2020. This work was supported in part by the Natural Science Foundation of China under Grant 61471295, in part by the Aeronautical Science Foundation of China under Grant 20172053017, and in part by the Central University Funds under Grant G2016KY0308, Grant G2016KY0002, and Grant 17GH030144. *(Corresponding author: Junli Liang.)*

Junli Liang, Xuhui Fan, and Deyun Zhou are with the School of Electronics and Information, Northwestern Polytechnical University, Xi'an 710072, China (e-mail: liangjunli@nwpu.edu.cn).

Hing Cheung So is with the Department of Electrical Engineering, City University of Hong Kong, Hong Kong.

Color versions of one or more of the figures in this article are available online at http://ieeexplore.ieee.org.

Digital Object Identifier 10.1109/TAP.2020.2972331

least-squares optimization problem of a single-modulus variable.

Notation: Vectors and matrices are denoted by boldface lowercase and uppercase letters, respectively. The $\|\cdot\|$ denotes the Frobenius norm, while $(\cdot)^T$, $(\cdot)^*$, $(\cdot)^H$, and $(\cdot)^{-1}$ are the transpose, conjugate, conjugate transpose, and matrix inverse operators, respectively. The $\mathbf{0}_{m\times n}$ and $\mathbf{I}_n$ represent the $m \times n$ zero matrix and $n \times n$ identity matrix, respectively. $\Re\{\}$ and $\Im\{\}$ mean the real and imaginary parts with $j = \sqrt{-1}$. $|\cdot|$ and $\angle\{\cdot\}$ are the magnitude and phase of a complex-valued scalar, respectively.

II. Problem Formulation

Consider a linear array with N antenna elements placed on known locations $l_n \in \mathcal{R}$ for $n = 1, \ldots, N$. The far-field radiated beampattern in the direction θ can be expressed as

$$\mathbf{w}^H\mathbf{a}(\theta)$$

where $\mathbf{w} = [w_1 \ldots w_N]^T$ and $\mathbf{a}(\theta) = [a_1(\theta) \ldots a_N(\theta)]^T$ denote, respectively, the complex (magnitude and phase) excitation vector and steering vector [2], [4], [13], [16]. Besides, the nth element $a_n(\theta)$ of $\mathbf{a}(\theta)$ is given by $\exp\{j(2\pi l_n \sin\theta)/\lambda\}$ where λ is the wavelength [2], [4], [13], [16]. It is worth pointing out: 1) although we describe only 1-D pattern synthesis problems here (i.e., linear arrays), their extensions to 2-D pattern synthesis problems are straightforward by replacing the 1-D steering vectors $\mathbf{a}(\theta)$ with the corresponding 2-D counterparts (i.e., planar arrays) and 2) although we describe the pattern synthesis problems with a common steering vector here (see [2, eq. (1)], [4, eq. (1)], [13, eq. (3)], [16, eq. (2)] for detail), their extensions to the mutual coupling case [35]–[38] and element radiation pattern-contained case (see [1, eq. (2)], [15, eq. (1)] for detail) are also obtained by replacing the steering vector with the corresponding counterparts.

Commonly, the mainlobe level U, the mainlobe ripple term η, and the sidelobe level Q [2], [4], [13], [15], [16] are given to specify the lobe level masks for beampattern synthesis, that is

$$\begin{cases} U-\eta \le |\mathbf{w}^H\mathbf{a}(\theta)|^2 \le U+\eta, & \theta \in \text{Mainlobe Region} \\ |\mathbf{w}^H\mathbf{a}(\theta)|^2 \le Q, & \theta \in \text{Sidelobe Region.} \end{cases} \tag{1}$$

However, when the given mainlobe level is excessively large or the specified sidelobe level is too small, a valid solution may not be obtained, especially for phase-only [16]–[21] and constant modulus pattern synthesis problems [21], [22], where there are finite degrees-of-freedom for the weight vector. With the typical considerations that the mainlobe level is expected to be as large as possible and the sidelobe level is anticipated to be as small as possible to suppress the interferences [1], [2], [15], we formulate the following beampattern synthesis model to avoid specifying a possibly improper or infeasible pattern mask from the feasibility viewpoint:

$$\begin{aligned} \min_{\mathbf{w}} \quad & \frac{\max_{\bar{\theta}_s} |\mathbf{w}^H\mathbf{a}(\bar{\theta}_s)|^2}{\min_{\theta_m} |\mathbf{w}^H\mathbf{a}(\theta_m)|^2} \\ \text{s.t.} \quad & \mathbf{w}^H\mathbf{w} = 1. \end{aligned} \tag{2}$$

Note that unlike (1), (2) does not need the knowledge of the lobe masks $\{U, Q, \eta\}$. In addition, considering that there are infinite solutions to such an optimization problem without constraints, i.e., $\min_{\mathbf{w}}[(\max_{\bar{\theta}_s}|\mathbf{w}^H\mathbf{a}(\bar{\theta}_s)|^2)/(\min_{\theta_m}|\mathbf{w}^H\mathbf{a}(\theta_m)|^2)]$, we add a norm constraint $\mathbf{w}^H\mathbf{w} = 1$ in (2) to avoid the scaling ambiguity issue. Moreover, the main beam angular region is divided into M uniformly spaced angles, i.e., $\{\theta_1, \ldots, \theta_M\}$, and the sidelobe angular region is divided into S uniformly spaced angles, i.e., $\{\bar{\theta}_1, \ldots, \bar{\theta}_S\}$. Obviously, (2) actually optimizes the amplitudes and phases of the complex weights $\{w_n\}_{n=1}^N$ since there is no magnitude or phase constraint on $\{w_n\}_{n=1}^N$.

In several applications, it is required to synthesize the phase-only [16]–[21] or constant modulus [21], [22] patterns, where the amplitudes are specified or fixed as the constant modulus. Thus, in such pattern synthesis problems, only the phases of the weights $\{w_n\}_{n=1}^N$ are required to be optimized. Since the phase-only synthesis problem may be transformed into the constant modulus synthesis problem (see Appendix A), we formulate only the constant modulus-constrained synthesis problem here

$$\begin{aligned} \min_{\mathbf{w}} \quad & \frac{\max_{\bar{\theta}_s} |\mathbf{w}^H\mathbf{a}(\bar{\theta}_s)|^2}{\min_{\theta_m} |\mathbf{w}^H\mathbf{a}(\theta_m)|^2} \\ \text{s.t.} \quad & |w_n| = 1, \quad n = 1, \ldots, N. \end{aligned} \tag{3}$$

Similar to [15] (see [15, eq. (16)] for details), we do not optimize the phases directly but consider the specified constant modulus (e.g., 1) as the constraints on the weights $\{w_n\}_{n=1}^N$ for computational purpose.

Our task is to solve the beampattern synthesis problems in (2) and (3) to obtain the weight vector $\mathbf{w}$ under the conditions that only the mainlobe and sidelobe angular regions are given, and that the mainlobe level, mainlobe ripple, and sidelobe level are not specified.

III. Proposed Method Without Magnitude Constraint

Although there is no magnitude constraint but norm constraint on the weight vector $\mathbf{w}$ in (2), the denominator and numerator are coupled in the objective function, and both are functions of $\mathbf{w}$. In particular, there are min and max operators in the denominator and numerator. All these make (2) difficult to tackle with.

To separate $\max_{\bar{\theta}_s} |\mathbf{w}^H\mathbf{a}(\bar{\theta}_s)|^2$ and $\min_{\theta_m} |\mathbf{w}^H\mathbf{a}(\theta_m)|^2$ in the fractional expression of (2), we define auxiliary exponent variables $\{p, q\}$, so that e^p and e^q act as the upper boundary of sidelobe levels and lower boundary of mainlobe levels, that is

$$\begin{aligned} |\mathbf{w}^H\mathbf{a}(\bar{\theta}_s)|^2 &\le e^p, \quad s = 1, \ldots, S \\ |\mathbf{w}^H\mathbf{a}(\theta_m)|^2 &\ge e^q, \quad m = 1, \ldots, M. \end{aligned} \tag{4}$$

In doing so, (2) can be rewritten as the following equivalent form:

$$\begin{aligned} \min_{\mathbf{w},p,q} \quad & e^{p-q} \\ \text{s.t.} \quad & |\mathbf{w}^H\mathbf{a}(\bar{\theta}_s)|^2 \le e^p, \quad s = 1, \ldots, S \\ & |\mathbf{w}^H\mathbf{a}(\theta_m)|^2 \ge e^q, \quad m = 1, \ldots, M \\ & \mathbf{w}^H\mathbf{w} = 1. \end{aligned} \tag{5}$$

Furthermore, minimization of e^{p-q} is equivalent to minimizing $p-q$, that is

$$\begin{aligned}\min_{\mathbf{w},p,q}\quad & p-q\\ \text{s.t. } & |\mathbf{w}^H\mathbf{a}(\bar{\theta}_s)|^2 \le e^p, \quad s=1,\ldots,S\\ & |\mathbf{w}^H\mathbf{a}(\theta_m)|^2 \ge e^q, \quad m=1,\ldots,M\\ & \mathbf{w}^H\mathbf{w}=1.\end{aligned} \tag{6}$$

Now the objective function becomes a linear function of p and q. However, the constraints $|\mathbf{w}^H\mathbf{a}(\bar{\theta}_s)|^2 \le e^p$ and $|\mathbf{w}^H\mathbf{a}(\theta_m)|^2 \ge e^q$ are coupled because they are all the functions of $\mathbf{w}$. To simplify the constraints, we introduce auxiliary variables

$$u_m = \mathbf{w}^H\mathbf{a}(\theta_m), \quad m=1,\ldots,M \tag{7}$$

and

$$v_s = \mathbf{w}^H\mathbf{a}(\bar{\theta}_s), \quad s=1,\ldots,S. \tag{8}$$

Then (6) becomes

$$\begin{aligned}\min_{\mathbf{w},\{u_m\},\{v_s\},p,q}\quad & p-q\\ \text{s.t. } & |u_m|^2 \ge e^q, \quad m=1,\ldots,M\\ & |v_s|^2 \le e^p, \quad s=1,\ldots,S\\ & u_m = \mathbf{w}^H\mathbf{a}(\theta_m), \quad m=1,\ldots,M\\ & v_s = \mathbf{w}^H\mathbf{a}(\bar{\theta}_s), \quad s=1,\ldots,S\\ & \mathbf{w}^H\mathbf{w}=1.\end{aligned} \tag{9}$$

Recently, the alternating direction method of multipliers (ADMM) (see Appendix B) [24]–[27] has received considerable attention due to its distinct decomposition–coordination procedure and superior convergence property [23], [28]–[31]. For this reason, we apply the ADMM to solve (9). Since the constraints $|u_m|^2 \ge e^q$ and $|v_s|^2 \le e^p$ will play their roles in the corresponding update step of variables q and p, respectively, we construct an augmented Lagrangian with constraints [24]–[27]

$$\begin{aligned}&\mathcal{L}_1(\mathbf{w},\mathbf{u},\mathbf{v},p,q,\boldsymbol{\lambda},\boldsymbol{\kappa})\\ &= p-q\\ &\quad+\sum_{m=1}^{M}\left(\Re\left\{\lambda_m^*(u_m-\mathbf{w}^H\mathbf{a}(\theta_m))\right\}+\frac{\rho}{2}|u_m-\mathbf{w}^H\mathbf{a}(\theta_m)|^2\right)\\ &\quad+\sum_{s=1}^{S}\left(\Re\left\{\kappa_s^*(v_s-\mathbf{w}^H\mathbf{a}(\bar{\theta}_s))\right\}+\frac{\rho}{2}|v_s-\mathbf{w}^H\mathbf{a}(\bar{\theta}_s)|^2\right)\\ &\quad\text{s.t. } |u_m|^2 \ge e^q, \quad m=1,\ldots,M\\ &\qquad\quad |v_s|^2 \le e^p, \quad s=1,\ldots,S\\ &\qquad\quad \mathbf{w}^H\mathbf{w}=1\end{aligned} \tag{10}$$

where $\rho>0$ is a user-defined step size [24], [25], and λ_m and κ_s are Lagrange multipliers corresponding to the constraints $u_m-\mathbf{w}^H\mathbf{a}(\theta_m)=0$ and $v_s-\mathbf{w}^H\mathbf{a}(\bar{\theta}_s)=0$, respectively, for $m=1,\ldots,M$ and $s=1,\ldots,S$. Note that $\mathbf{u}=[u_1\ldots u_M]^T$, $\mathbf{v}=[v_1\ldots v_S]^T$, $\boldsymbol{\lambda}=[\lambda_1\ldots\lambda_M]^T$, and $\boldsymbol{\kappa}=[\kappa_1\ldots\kappa_S]^T$.

Based on ADMM [24]–[27], we solve (10) via the following iterative steps.

Step 1: Update $\{\mathbf{u}(t+1),\mathbf{v}(t+1),p(t+1),q(t+1)\}$ with $\{\mathbf{w}(t),\boldsymbol{\lambda}(t),\boldsymbol{\kappa}(t)\}$ obtained in the $(t-1)$th iteration by solving the optimization problem

$$\begin{aligned}&\{\mathbf{u}(t+1),\mathbf{v}(t+1),p(t+1),q(t+1)\}\\ &=\arg\min_{\mathbf{u},\mathbf{v},p,q}\mathcal{L}_1(\mathbf{w}(t),\mathbf{u},\mathbf{v},p,q,\boldsymbol{\lambda}(t),\boldsymbol{\kappa}(t))\\ &=\arg\min_{\mathbf{u},\mathbf{v},p,q}\quad p-q\\ &\quad+\sum_{m=1}^{M}\left(\Re\{\lambda_m^*(t)(u_m-\mathbf{w}^H(t)\mathbf{a}(\theta_m))\}\right.\\ &\qquad\left.+\frac{\rho}{2}|u_m-\mathbf{w}^H(t)\mathbf{a}(\theta_m)|^2\right)\\ &\quad+\sum_{s=1}^{S}\left(\Re\left\{\kappa_s^*(t)(v_s-\mathbf{w}^H(t)\mathbf{a}(\bar{\theta}_s))\right\}\right.\\ &\qquad\left.+\frac{\rho}{2}|v_s-\mathbf{w}^H(t)\mathbf{a}(\bar{\theta}_s)|^2\right)\\ &\quad\text{s.t. } |u_m|^2 \ge e^q, \quad m=1,\ldots,M\\ &\qquad\quad |v_s|^2 \le e^p, \quad s=1,\ldots,S\end{aligned} \tag{11}$$

where t denotes the number of iterations.

Ignoring the irrelevant terms and completing the square, we are able to express (11) in a compact form as

$$\begin{aligned}\min_{\mathbf{u},\mathbf{v},p,q}\quad & p-q+\frac{\rho}{2}\sum_{m=1}^{M}|u_m-x_m|^2+\frac{\rho}{2}\sum_{s=1}^{S}|v_s-y_s|^2\\ \text{s.t.}\quad & |u_m|^2 \ge e^q, \quad m=1,\ldots,M\\ & |v_s|^2 \le e^p, \quad s=1,\ldots,S\end{aligned} \tag{12}$$

where

$$x_m = \mathbf{w}^H(t)\mathbf{a}(\theta_m)-\frac{1}{\rho}\lambda_m(t), \quad m=1,\ldots,M \tag{13}$$

$$y_s = \mathbf{w}^H(t)\mathbf{a}(\bar{\theta}_s)-\frac{1}{\rho}\kappa_s(t), \quad s=1,\ldots,S \tag{14}$$

for $m=1,\ldots,M$ and $s=1,\ldots,S$, which can be divided into two subproblems, respectively, with variables $\{\mathbf{v},p\}$ and $\{\mathbf{u},q\}$

$$\begin{aligned}\min_{\mathbf{v},p}\quad & p+\frac{\rho}{2}\sum_{s=1}^{S}|v_s-y_s|^2\\ \text{s.t.}\quad & |v_s|^2 \le e^p, \quad s=1,\ldots,S\end{aligned} \tag{15}$$

and

$$\begin{aligned}\min_{\mathbf{u},q}\quad & -q+\frac{\rho}{2}\sum_{m=1}^{M}|u_m-x_m|^2\\ \text{s.t.}\quad & |u_m|^2 \ge e^q, \quad m=1,\ldots,M.\end{aligned} \tag{16}$$

However, the two subproblems are still difficult to solve [32], [33] due to the coupled variables $\{v_s\}$ and p as well as $\{u_m\}$ and q. Here we consider transforming the subproblems of coupled variables into optimization problems of a single variable in order to tackle them easily.

If $\{p,q\}$ are known, the optimal $u_m(t+1)$ is expressed in terms of q

$$u_m(t+1)=\begin{cases}e^{\frac{q}{2}}\exp\{j\angle x_m\}, & \text{if } |x_m|\le e^{\frac{q}{2}}\\ x_m, & \text{otherwise}\end{cases} \tag{17}$$

for $m = 1, \ldots, M$, and the optimal $v_s(t+1)$ is represented in terms of p as

$$v_s(t+1) = \begin{cases} e^{\frac{p}{2}} \exp\{j \angle y_s\}, & \text{if } |y_s| \geq e^{\frac{p}{2}} \\ y_s, & \text{otherwise} \end{cases} \tag{18}$$

for $s = 1, \ldots, S$.

With the parametric representation of $\{v_s\}$ in (18), we consider transforming (15) into an optimization problem of only p rather than $\{v_s\}$ and p. For this purpose, we define a unit-step function $S_1(y_s, p)$ [28]

$$S_1(y_s, p) = \begin{cases} 1, & \text{if } |y_s| \geq e^{\frac{p}{2}} \\ 0, & \text{otherwise.} \end{cases} \tag{19}$$

Combining the unit-step function and (18), we rewrite (15) as a single variable problem

$$\min_p \; p + \frac{\rho}{2} \sum_{s=1}^{S} S_1(y_s, p) \times (e^{\frac{p}{2}} - |y_s|)^2 \tag{20}$$

which shows that the part $\rho/2 \sum_{s=1}^{S} S_1(y_s, p) \times (e^{(p/2)} - |y_s|)^2$ in (20) depends on the value of p.

Setting $e^{(p/2)} - |y_s|$ to zero yields the solution $p = 2 \ln |y_s|$ for $s = 1, \ldots, S$, from which we select the reasonable turning points within a prior region (p_L, p_U) denoted by $\{p_1(t+1), \ldots, p_K(t+1)\}$ in ascending order, where $K \leq S$. Thus, we divide the region $[p_L, p_U]$ into $(K+1)$ subregions, i.e., $[p_L, p_1(t+1)]$, $[p_1(t+1), p_2(t+1)]$, $\ldots$, $[p_K(t+1), p_U]$. In each subregion, there are concrete values for the unit-step functions $S_1(y_s, p)$ for $s = 1, \ldots, S$, which implies that the objective function in (20) has different representations in the $(K+1)$ subregions and thus, (20) is actually a piecewise function.

For the kth segment, i.e., $p \in [p_{k-1}(t+1), p_k(t+1)]$, the objective function in (20) is rewritten as

$$f(p) = p + A_k \left(e^{\frac{p}{2}} - \frac{B_k}{2A_k} \right)^2 + C_k - \frac{B_k^2}{4A_k} \tag{21}$$

for $k = 1, \ldots, K+1$, where $C_k - \frac{B_k^2}{4A_k}$ is a constant term, and A_k, B_k, and C_k are given by

$$A_k = \frac{\rho}{2} \sum_{s=1}^{S} S_1(y_s, p) > 0 \tag{22}$$

$$B_k = \rho \sum_{s=1}^{S} S_1(y_s, p) |y_s| > 0 \tag{23}$$

$$C_k = \frac{\rho}{2} \sum_{s=1}^{S} S_1(y_s, p) |y_s|^2 > 0. \tag{24}$$

Now we discuss the convexity or concavity [32], [33] of $f(p)$ in the subregion $[p_{k-1}(t+1), p_k(t+1)]$ in terms of its first- and second-order derivatives

$$\frac{df(p)}{dp} = 1 + A_k e^{\frac{p}{2}} \left(e^{\frac{p}{2}} - \frac{B_k}{2A_k} \right) \tag{25}$$

$$\frac{d^2 f(p)}{dp^2} = A_k e^{\frac{p}{2}} \left(e^{\frac{p}{2}} - \frac{B_k}{4A_k} \right). \tag{26}$$

Since $e^{(p)/(2)} > 0$ in the region $[p_{k-1}(t+1), p_k(t+1)]$, the sign of $(d^2 f(p)/dp^2)$ depends on the term $(e^{(p/2)} - (B_k/4A_k))$. Then we consider the following three cases according to the relationship between $2\ln(B_k/4A_k)$ and the region $[p_{k-1}(t+1), p_k(t+1)]$.

Case A $2\ln(B_k/4A_k) \leq p_{k-1}(t+1)$: In this case, $(e^{(p/2)} - (B_k/4A_k)) \geq 0$ in the region, $f(p)$ is convex in this region, and $(df(p)/dp)$ increases with p in the region $[p_{k-1}(t+1), p_k(t+1)]$. Thus, we determine the minimum from the following three subcases.

Case A-i $(df(p)/dp)|_{p=p_{k-1}(t+1)} \geq 0$: The minimum of the piecewise function $f(p)$ in the region $[p_{k-1}(t+1), p_k(t+1)]$ attains at $p = p_{k-1}(t+1)$.

Case A-ii $(df(p)/dp)|_{p=p_k(t+1)} \leq 0$: The minimum of the piecewise function $f(p)$ in the region $[p_{k-1}(t+1), p_k(t+1)]$ attains at $p = p_k(t+1)$.

Case A-iii Otherwise: We apply a simple bisection method to obtain the minimum by finding the root of the nonlinear equation $(df(p)/dp) = 1 + A_k e^{(p)/(2)}(e^{(p)/(2)} - (B_k)/(2A_k)) = 0$ in the region $[p_{k-1}(t+1), p_k(t+1)]$.

Case B $2\ln(B_k/4A_k) \geq p_k(t+1)$: In this case, $(e^{(p/2)} - (B_k/4A_k) \leq 0$ in the region, $f(p)$ is concave in the region $[p_{k-1}(t+1), p_k(t+1)]$. Thus, we determine the minimum by comparing the function values at the boundary points of the region $[p_{k-1}(t+1), p_k(t+1)]$.

Case C $p_{k-1}(t+1) \leq 2\ln(B_k/4A_k) \leq p_k(t+1)$: We divide the region $[p_{k-1}(t+1), p_k(t+1)]$ into two parts, i.e., $[p_{k-1}(t+1), 2\ln(B_k/4A_k)]$ and $[2\ln(B_k/4A_k), p_k(t+1)]$, and select the final minimum from the local minima in the two subregions.

Case C-i In the subregion $[p_{k-1}(t+1), 2\ln(B_k/4A_k)]$: the minimum in the subregion is obtained in the similar manner as **Case B**.

Case C-ii In the subregion $[2\ln(B_k/4A_k), p_k(t+1)]$: the minimum in the subregion is obtained in the similar manner as **Case A**.

Thus, from the aforementioned discussion, we derive the optimal value p and objective function values $f(p)$ in the subregion $[p_{k-1}(t+1), p_k(t+1)]$ for $k = 1, \ldots, K+1$. By selecting the smallest one (global minimum) from all the $(K+1)$ objective function values ($K+1$ locally minima), we pick out the optimal $\breve{p}$ in the feasible region $[p_L, p_U]$, denoted as $p(t+1)$.

Similar to (19), we define another unit-step function $S_2(x_m, q)$

$$S_2(x_m, q) = \begin{cases} 1, & \text{if } |x_m| \leq e^{\frac{q}{2}} \\ 0, & \text{otherwise} \end{cases} \tag{27}$$

for q, and thus we rewrite (16) as

$$\min_q \; -q + \sum_{m=1}^{M} S_2(x_m, q) \times (e^{\frac{q}{2}} - |x_m|)^2. \tag{28}$$

Similar to (20), we can get the optimal $\breve{q}$ as $q(t+1)$ from (28). Then substituting $q(t+1)$ and $p(t+1)$ into (17) and (18) yield $u_m(t+1)$ and $v_s(t+1)$, respectively.

Step 2: Update $\mathbf{w}(t+1)$ with given $\{\boldsymbol{\lambda}(t), \boldsymbol{\kappa}(t)\}$ and $\{\mathbf{u}(t+1), \mathbf{v}(t+1), p(t+1), q(t+1)\}$ by solving

$$\begin{aligned}
&\mathbf{w}(t+1)\\
&= \arg\min_{\mathbf{w}}\\
&\quad \times \mathcal{L}_1(\mathbf{w}, \mathbf{u}(t+1), \mathbf{v}(t+1), p(t+1), q(t+1), \boldsymbol{\lambda}(t), \boldsymbol{\kappa}(t))\\
&= \arg\min_{\mathbf{w}} \sum_{m=1}^{M} \left| u_m(t+1) + \frac{\lambda_m(t)}{\rho} - \mathbf{w}^H \mathbf{a}(\theta_m) \right|^2\\
&\quad + \sum_{s=1}^{S} \left| v_s(t+1) + \frac{\kappa_s(t)}{\rho} - \mathbf{w}^H \mathbf{a}(\bar{\theta}_s) \right|^2\\
&\quad \text{s.t.} \quad \mathbf{w}^H \mathbf{w} = 1
\end{aligned} \tag{29}$$

which can be represented in a compact form as

$$\begin{aligned}
&\min_{\mathbf{w}} \quad \mathbf{w}^H \mathbf{R} \mathbf{w} + \mathbf{b}^H \mathbf{w} + \mathbf{w}^H \mathbf{b}\\
&\text{s.t.} \quad \mathbf{w}^H \mathbf{w} = 1
\end{aligned} \tag{30}$$

where

$$\mathbf{R} = \sum_{m=1}^{M} \mathbf{a}(\theta_m)\mathbf{a}^H(\theta_m) + \sum_{s=1}^{S} \mathbf{a}(\bar{\theta}_s)\mathbf{a}^H(\bar{\theta}_s) \tag{31}$$

and

$$\begin{aligned}
\mathbf{b} = &- \sum_{m=1}^{M} \left(u_m(t+1) + \frac{\lambda_m(t)}{\rho} \right)^* \mathbf{a}(\theta_m)\\
&- \sum_{s=1}^{S} \left(v_s(t+1) + \frac{\kappa_s(t)}{\rho} \right)^* \mathbf{a}(\bar{\theta}_s).
\end{aligned} \tag{32}$$

Then we define the Lagrangian for (30) as [32], [33]

$$\mathcal{F}(\mathbf{w}, \lambda) = \mathbf{w}^H \mathbf{R} \mathbf{w} + \mathbf{b}^H \mathbf{w} + \mathbf{w}^H \mathbf{b} + \lambda(\mathbf{w}^H \mathbf{w} - 1). \tag{33}$$

Partial differentiating $\mathcal{F}(\mathbf{w}, \lambda)$ with respect to $\mathbf{w}$ and λ, respectively, and setting the results to zero yield the so-called two Lagrange equations [32], [33], that is

$$2\mathbf{R}\mathbf{w} + 2\mathbf{b} + 2\lambda\mathbf{w} = 0 \tag{34}$$

and $\mathbf{w}^H \mathbf{w} = 1$. From (34) we derive the analytical solution

$$\mathbf{w} = -(\mathbf{R} + \lambda \mathbf{I}_N)^{-1} \mathbf{b} \tag{35}$$

by noting $\mathbf{w}^H \mathbf{w} = 1$. We also derive the function of the Lagrange multiplier λ as

$$g(\lambda) = \mathbf{b}^H (\mathbf{R} + \lambda \mathbf{I}_N)^{-2} \mathbf{b} - 1 \tag{36}$$

which shows that the optimal value $\breve{\lambda}$ is the root of $g(\lambda) = 0$ [32], [33].

We implement the eigenvalue decomposition of $\mathbf{R}$ as

$$\mathbf{R} = \mathbf{U} \Sigma \mathbf{U}^H \tag{37}$$

where $\Sigma = \text{diag}\{\sigma_1, \sigma_2, \ldots, \sigma_N\}$ is the diagonal eigenvalue matrix and the eigenvalues are arranged in the descending order, i.e., $\sigma_1 \geq \sigma_2 \geq \cdots \geq \sigma_N \geq 0$. In addition, the corresponding eigenvectors $\{\mathbf{u}_n\}$ form the eigenvector matrix $\mathbf{U} = [\mathbf{u}_1\ \mathbf{u}_2 \ldots \mathbf{u}_N]$.

Thus,

$$\begin{aligned}
g(\lambda) &= \mathbf{b}^H \mathbf{U} (\Sigma + \lambda \mathbf{I}_N)^{-2} \mathbf{U}^H \mathbf{b} - 1\\
&= \sum_{n=1}^{N} \frac{|\mathbf{b}^H \mathbf{u}_n|^2}{(\sigma_n + \lambda)^2} - 1.
\end{aligned} \tag{38}$$

Since $\lim_{\lambda \to -\sigma_N} g(\lambda) = +\infty$ and $\lim_{\lambda \to +\infty} g(\lambda) = -1$, and

$$\frac{\partial g(\lambda)}{\partial \lambda} = \sum_{n=1}^{N} -2\frac{|\mathbf{b}^H \mathbf{u}_n|^2}{(\sigma_n + \lambda)^3} < 0, \quad \text{for} \quad \lambda \in (-\sigma_N, +\infty) \tag{39}$$

$g(\lambda)$ is a monotonically decreasing function [32] and thus, there is a unique solution $\breve{\lambda}$ to $g(\lambda) = 0$ in the region $\lambda \in (-\sigma_N, +\infty)$. Therefore, we can determine the Lagrange multiplier $\breve{\lambda}$ by a simple bisection method and insert it into (35) to yield $\mathbf{w}(t+1)$.

Step 3: Update Lagrange multipliers $\{\kappa_s(t+1), \lambda_m(t+1)\}$ as

$$\kappa_s(t+1) = \kappa_s(t) + \rho(v_s(t+1) - \mathbf{w}^H(t+1)\mathbf{a}(\tilde{\theta}_s)) \tag{40}$$

$$\lambda_m(t+1) = \lambda_m(t) + \rho(u_m(t+1) - \mathbf{w}^H(t+1)\mathbf{a}(\theta_m)) \tag{41}$$

for $m = 1, \ldots, M$ and $s = 1, \ldots, S$.

Steps 1–3 are repeated until a predefined maximum iteration number T or both $\max_m |u_m - \mathbf{w}^H \mathbf{a}(\theta_m)| \leq 10^{-4}$ and $\max_s |v_s - \mathbf{w}^H \mathbf{a}(\bar{\theta}_s)| \leq 10^{-4}$ are reached.

Based on Steps 1–3, the proposed beampattern synthesis method without magnitude constraints is summarized in Algorithm 1.

Algorithm 1 Beampattern Synthesis Without Magnitude Constraints

Initialization: $\{\boldsymbol{\lambda}(0), \boldsymbol{\kappa}(0), \mathbf{w}(0)\}$, and T;
for $t = 0, \ldots, T$
Obtain p and $\{v_s(t+1)\}$ using the steps in (18)-(26);
Obtain q and $\{u_m(t+1)\}$ using the steps in (17) and (27)-(28);
Determine $\mathbf{w}(t+1)$ using the steps in (29)-(39);
Update $\{\boldsymbol{\lambda}(t+1), \boldsymbol{\kappa}(t+1)\}$ using (40)-(41);
end for $t = T$ or both $\max_m |u_m - \mathbf{w}^H \mathbf{a}(\theta_m)| \leq 10^{-4}$ and $\max_s |v_s - \mathbf{w}^H \mathbf{a}(\bar{\theta}_s)| \leq 10^{-4}$ are satisfied.
Output $\mathbf{w}_{opt}$.

IV. Extension to Constant Modulus Synthesis

Since the phase-only [16]–[20] synthesis problem may be transformed into the constant modulus [21], [22] synthesis problem, we only discuss how to solve the constant modulus [21], [22] synthesis problem in this section.

Similar to (4) and (5), we transform (3) as the following equivalent problem:

$$\begin{aligned}
&\min_{\mathbf{w}, p, q} \quad e^{p-q}\\
&\text{s.t.} \quad |\mathbf{w}^H \mathbf{a}(\bar{\theta}_s)|^2 \leq e^p, \quad s = 1, \ldots, S\\
&\qquad |\mathbf{w}^H \mathbf{a}(\theta_m)|^2 \geq e^q, \quad m = 1, \ldots, M\\
&\qquad |w_n| = 1, \quad n = 1, \ldots, N.
\end{aligned} \tag{42}$$

Next we define

$$\tilde{p} = e^{p-q} \tag{43}$$

$$\tilde{w}_n = \frac{w_n}{e^{\frac{q}{2}}} \tag{44}$$

$$\xi = \frac{1}{e^{\frac{q}{2}}}. \tag{45}$$

Then (42) is equivalent to

$$\begin{aligned}\min_{\tilde{\mathbf{w}},\tilde{p},\xi}\quad & \tilde{p}\\ \text{s.t.}\quad & |\tilde{\mathbf{w}}^H\mathbf{a}(\bar{\theta}_s)|^2\le\tilde{p},\quad s=1,\ldots,S\\ & |\tilde{\mathbf{w}}^H\mathbf{a}(\theta_m)|^2\ge 1,\quad m=1,\ldots,M\\ & |\tilde{w}_n|=\xi,\quad n=1,\ldots,N\end{aligned}\tag{46}$$

where $\tilde{\mathbf{w}}=[\tilde{w}_1,\ldots,\tilde{w}_N]^T$. Note that two kinds of nonconvex constraints $|\tilde{\mathbf{w}}^H\mathbf{a}(\theta_m)|^2\ge 1$ and $|\tilde{w}_n|=\xi$ are coupled and it is not easy to solve (46). To separate the two kinds of constraints and simplify the optimization problem, we introduce the auxiliary vector $\mathbf{z}$ with the constraint $\tilde{\mathbf{w}}=\mathbf{z}$. Then we have the following equivalent optimization problem:

$$\begin{aligned}\min_{\tilde{\mathbf{w}},\mathbf{z},\tilde{p},\xi}\quad & \tilde{p}\\ \text{s.t.}\quad & |\tilde{\mathbf{w}}^H\mathbf{a}(\bar{\theta}_s)|^2\le\tilde{p},\quad s=1,\ldots,S\\ & |\tilde{\mathbf{w}}^H\mathbf{a}(\theta_m)|^2\ge 1,\quad m=1,\ldots,M\\ & \tilde{\mathbf{w}}=\mathbf{z};\\ & |z_n|=\xi,\quad n=1,\ldots,N.\end{aligned}\tag{47}$$

Similarly, we define $\tilde{u}_m=\tilde{\mathbf{w}}^H\mathbf{a}(\theta_m)$ and $\tilde{v}_s=\tilde{\mathbf{w}}^H\mathbf{a}(\bar{\theta}_s)$, and construct another augmented Lagrangian style formulation [24]–[27] as follows:

$$\begin{aligned}&\mathcal{L}_2(\tilde{\mathbf{w}},\mathbf{z},\tilde{\mathbf{u}},\tilde{\mathbf{v}},\tilde{p},\tilde{\boldsymbol{\lambda}},\tilde{\boldsymbol{\kappa}},\tilde{\boldsymbol{\gamma}})\\ &=\tilde{p}\\ &\quad+\sum_{m=1}^{M}\left(\Re\left\{\tilde{\lambda}_m^*(\tilde{u}_m-\tilde{\mathbf{w}}^H\mathbf{a}(\theta_m))\right\}+\frac{\rho}{2}|\tilde{u}_m-\tilde{\mathbf{w}}^H\mathbf{a}(\theta_m)|^2\right)\\ &\quad+\sum_{s=1}^{S}\left(\Re\left\{\tilde{\kappa}_s^*(\tilde{v}_s-\tilde{\mathbf{w}}^H\mathbf{a}(\bar{\theta}_s))\right\}+\frac{\rho}{2}|\tilde{v}_s-\tilde{\mathbf{w}}^H\mathbf{a}(\bar{\theta}_s)|^2\right)\\ &\quad+\Re\left\{\tilde{\boldsymbol{\gamma}}^H(\tilde{\mathbf{w}}-\mathbf{z})\right\}+\frac{\rho}{2}|\tilde{\mathbf{w}}-\mathbf{z}|^2\\ &\quad\text{s.t. }|\tilde{u}_m|^2\ge 1,\quad m=1,\ldots,M\\ &\qquad|\tilde{v}_s|^2\le\tilde{p},\quad s=1,\ldots,S\\ &\qquad|z_n|=\xi,\quad n=1,\ldots,N\end{aligned}\tag{48}$$

where $\tilde{\lambda}_m$ and $\tilde{\kappa}_s$ are Lagrange multipliers corresponding to the constraints $\tilde{u}_m-\tilde{\mathbf{w}}^H\mathbf{a}(\theta_m)=0$ and $\tilde{v}_s-\tilde{\mathbf{w}}^H\mathbf{a}(\bar{\theta}_s)=0$, respectively, for $m=1,\ldots,M$ and $s=1,\ldots,S$. Additionally, $\tilde{\boldsymbol{\gamma}}=[\tilde{\gamma}_1\ \tilde{\gamma}_2\ \ldots\ \tilde{\gamma}_N]^T$ is the Lagrange multiplier vector corresponding to the constraint $\tilde{\mathbf{w}}=\mathbf{z}$, and $\tilde{\mathbf{u}}=[\tilde{u}_1\ldots\tilde{u}_M]^T$, $\tilde{\mathbf{v}}=[\tilde{v}_1\ldots\tilde{v}_S]^T$, $\tilde{\boldsymbol{\lambda}}=[\tilde{\lambda}_1\ldots\tilde{\lambda}_M]^T$ and $\tilde{\boldsymbol{\kappa}}=[\tilde{\kappa}_1\ldots\tilde{\kappa}_S]^T$.

Based on ADMM [24]–[27], we solve (48) via the following iterative steps.

Step 1: Update $\{\tilde{\mathbf{u}}(t+1),\tilde{\mathbf{v}}(t+1),\tilde{p}(t+1),\mathbf{z}(t+1)\}$ with given $\{\tilde{\boldsymbol{\lambda}}(t),\tilde{\boldsymbol{\kappa}}(t),\tilde{\boldsymbol{\gamma}}(t)\}$, and $\tilde{\mathbf{w}}(t)$ by solving the optimization problem

$$\begin{aligned}&\{\tilde{\mathbf{u}}(t+1),\tilde{\mathbf{v}}(t+1),\tilde{p}(t+1),\mathbf{z}(t+1)\}\\ &=\arg\min_{\tilde{\mathbf{u}},\tilde{\mathbf{v}},\tilde{p},\mathbf{z}}\mathcal{L}_2(\tilde{\mathbf{w}}(t),\mathbf{z},\tilde{\mathbf{u}},\tilde{\mathbf{v}},\tilde{p},\tilde{\boldsymbol{\lambda}}(t),\tilde{\boldsymbol{\kappa}}(t),\tilde{\boldsymbol{\gamma}}(t))\\ &=\tilde{p}+\sum_{m=1}^{M}\left(\Re\{\tilde{\lambda}_m^*(t)(\tilde{u}_m-\tilde{\mathbf{w}}^H(t)\mathbf{a}(\theta_m))\}\right.\\ &\qquad\left.+\frac{\rho}{2}|\tilde{u}_m-\tilde{\mathbf{w}}^H(t)\mathbf{a}(\theta_m)|^2\right)\\ &\quad+\sum_{s=1}^{S}\left(\Re\{\tilde{\kappa}_s^*(t)(\tilde{v}_s-\tilde{\mathbf{w}}^H(t)\mathbf{a}(\bar{\theta}_s))\}\right.\\ &\qquad\left.+\frac{\rho}{2}|\tilde{v}_s-\tilde{\mathbf{w}}^H(t)\mathbf{a}(\bar{\theta}_s)|^2\right)\\ &\quad+\Re\{\tilde{\boldsymbol{\gamma}}^H(t)(\tilde{\mathbf{w}}(t)-\mathbf{z})\}+\frac{\rho}{2}|\tilde{\mathbf{w}}(t)-\mathbf{z}|^2\\ &\quad\text{s.t. }|\tilde{u}_m|^2\ge 1,\quad m=1,\ldots M\\ &\qquad|\tilde{v}_s|^2\le\tilde{p},\quad s=1,\ldots,S\\ &\qquad|z_n|=\xi,\quad n=1,\ldots,N\end{aligned}\tag{49}$$

which can be divided into the following three subproblems:

$$\begin{aligned}\min_{\mathbf{z},\xi}\quad & \Re\{\tilde{\boldsymbol{\gamma}}^H(t)(\tilde{\mathbf{w}}(t)-\mathbf{z})\}+\frac{\rho}{2}|\tilde{\mathbf{w}}(t)-\mathbf{z}|^2\\ \text{s.t.}\quad & |z_n|=\xi,\quad n=1,\ldots,N\end{aligned}\tag{50}$$

$$\begin{aligned}\min_{\tilde{u}_m}\quad & \sum_{m=1}^{M}\left(\Re\{\tilde{\lambda}_m^*(t)(\tilde{u}_m-\tilde{\mathbf{w}}^H(t)\mathbf{a}(\theta_m))\}\right.\\ &\left.+\frac{\rho}{2}|\tilde{u}_m-\tilde{\mathbf{w}}^H(t)\mathbf{a}(\theta_m)|^2\right)\\ \text{s.t.}\quad & |\tilde{u}_m|^2\ge 1,\quad m=1,\ldots,M\end{aligned}\tag{51}$$

and

$$\begin{aligned}\min_{\tilde{v}_s,\tilde{p}}\quad & \tilde{p}+\sum_{s=1}^{S}\left(\Re\{\tilde{\kappa}_s^*(t)(\tilde{v}_s-\tilde{\mathbf{w}}^H(t)\mathbf{a}(\bar{\theta}_s))\}\right.\\ &\left.+\frac{\rho}{2}|\tilde{v}_s-\tilde{\mathbf{w}}^H(t)\mathbf{a}(\bar{\theta}_s)|^2\right)\\ \text{s.t.}\quad & |\tilde{v}_s|^2\le\tilde{p},\quad s=1,\ldots,S.\end{aligned}\tag{52}$$

Obviously, the first subproblem in (50) is equivalent to

$$\begin{aligned}\min_{\mathbf{z},\xi}\quad & \sum_{n=1}^{N}\left|\tilde{w}_n(t)+\frac{\tilde{\gamma}_n(t)}{\rho}-z_n\right|^2\\ \text{s.t.}\quad & |z_n|=\xi,\quad n=1,\ldots,N\end{aligned}\tag{53}$$

where $\tilde{w}_n$ and $\tilde{\gamma}_n$ are the nth entries of $\tilde{\mathbf{w}}$ and $\tilde{\boldsymbol{\gamma}}$, respectively, for $n=1,\ldots,N$. Here we consider transforming the optimization problem of both $\mathbf{z}$ and ξ into a problem of a single-variable ξ to simplify the computation. When ξ is known, the optimal $z_n(t+1)$ is given by

$$z_n(t+1)=\xi\exp\left\{\sqrt{-1}\angle(\tilde{w}_n(t)+\frac{\tilde{\gamma}_n(t)}{\rho})\right\}.\tag{54}$$

Substituting (54) into (53) yields an optimization problem of a single-variable ξ

$$\min_{\xi}\quad\sum_{n=1}^{N}\quad\left(|\tilde{w}_n(t)+\frac{\tilde{\gamma}_n(t)}{\rho}|-\xi\right)^2\tag{55}$$

whose solution is given by

$$\xi(t+1)=\frac{1}{N}\sum_{n=1}^{N}\left|\tilde{w}_n(t)+\frac{\tilde{\gamma}_n(t)}{\rho}\right|.\tag{56}$$

Thus, substituting (56) into (54) yields the optimal $z_n(t+1)$ with the known $\xi(t+1)$.

Note that the solution to the second subproblem in (51) is easily derived as

$$\tilde{u}_m(t+1) = \begin{cases} \dfrac{\tilde{\mathbf{w}}^H(t)\mathbf{a}(\theta_m) - \dfrac{\tilde{\lambda}_m(t)}{\rho}}{\left|\tilde{\mathbf{w}}^H(t)\mathbf{a}(\theta_m) - \dfrac{\tilde{\lambda}_m(t)}{\rho}\right|} & \text{if } \left|\tilde{\mathbf{w}}^H(t)\mathbf{a}(\theta_m) - \dfrac{\tilde{\lambda}_m(t)}{\rho}\right| < 1 \\ \tilde{\mathbf{w}}^H(t)\mathbf{a}(\theta_m) - \dfrac{\tilde{\lambda}_m(t)}{\rho} & \text{otherwise.} \end{cases} \quad (57)$$

For the third subproblem shown in (52), we define the unit-step function $S_3(\tilde{y}_s, \tilde{p})$ [28]

$$S_3(\tilde{y}_s, \tilde{p}) = \begin{cases} 1, & \text{if } |\tilde{y}_s|^2 \geq \tilde{p} \\ 0, & \text{otherwise} \end{cases} \quad (58)$$

where

$$\tilde{y}_s = \tilde{\mathbf{w}}^H(t)\mathbf{a}(\bar{\theta}_s) - \frac{\tilde{\kappa}_s(t)}{\rho}, \quad s = 1, \ldots, S. \quad (59)$$

With $S_3(\tilde{v}_s, \tilde{p})$, we rewrite (52) as

$$\min_{\tilde{p}} \ \tilde{p} + \frac{\rho}{2}\sum_{s=1}^{S} S_3(\tilde{y}_s, \tilde{p}) \times (\sqrt{\tilde{p}} - |\tilde{y}_s|)^2 \quad (60)$$

which implies that the part $(\rho/2)\sum_{s=1}^{S} S_3(\tilde{y}_s, \tilde{p}) \times (\sqrt{\tilde{p}} - |\tilde{y}_s|)^2$ in (60) depends on the value of $\tilde{p}$. From the turning points $\{|\tilde{y}_1|^2, |\tilde{y}_2|^2, \ldots, |\tilde{y}_S|^2\}$ yielded from $\sqrt{\tilde{p}} = |\tilde{y}_s|$, we select the reasonable turning points which lie in the prior region $(\tilde{p}_L, \tilde{p}_U)$ denoted by $\{\tilde{p}_1(t+1), \ldots, \tilde{p}_K(t+1)\}$ arranged in ascending order. Then we divide the prior region $[\tilde{p}_L, \tilde{p}_U]$ into $K+1$ subregions $[\tilde{p}_L, \tilde{p}_1(t+1)]$, $[\tilde{p}_1(t+1), \tilde{p}_2(t+1)]$, $\ldots$, $[\tilde{p}_K(t+1), \tilde{p}_U]$. Thus, for each subregion there are concrete values for the unit-step functions. Especially, when $\tilde{p} \in [\tilde{p}_{k-1}(t+1), \tilde{p}_k(t+1)]$, the objective function in (60) has the following form:

$$g(\tilde{p}) = \tilde{A}_k\tilde{p} - \tilde{B}_k\sqrt{\tilde{p}} + \tilde{C}_k, \quad k = 1, \ldots, K+1 \quad (61)$$

where $\tilde{A}_k$, $\tilde{B}_k$, and $\tilde{C}_k$ are given by

$$\tilde{A}_k = 1 + \frac{\rho}{2}\sum_{s=1}^{S} S_3(\tilde{y}_s, \tilde{p}) > 0 \quad (62)$$

$$\tilde{B}_k = \rho\sum_{s=1}^{S} S_3(\tilde{y}_s, \tilde{p})|\tilde{y}_s| > 0 \quad (63)$$

$$\tilde{C}_k = \frac{\rho}{2}\sum_{s=1}^{S} S_3(\tilde{y}_s, \tilde{p})|\tilde{y}_s|^2 > 0. \quad (64)$$

It is clear that the local minimum $(\tilde{B}_k^2/4\tilde{A}_k^2)$ in the subregion $[\tilde{p}_{k-1}(t+1), \tilde{p}_k(t+1)]$ is attained at $\sqrt{\tilde{p}} = (\tilde{B}_k/2\tilde{A}_k)$. By selecting the globally smallest one from all the $(K+1)$ local minima of the $K+1$ subregions, we get the optimal value of $\tilde{p}$ as $\tilde{p}(t+1)$ in the feasible region $[\tilde{p}_L, \tilde{p}_U]$, corresponding to the globally smallest objective function value. Then with $\tilde{p}(t+1)$, $\tilde{v}_s(t+1)$ is updated as

$$\tilde{v}_s(t+1) = \begin{cases} \sqrt{\tilde{p}(t+1)}\exp\{\sqrt{-1}\angle(\tilde{y}_s)\}, & \text{if } |\tilde{y}_s|^2 \geq \tilde{p}(t+1) \\ \tilde{y}_s, & \text{otherwise.} \end{cases} \quad (65)$$

Step 2: Update $\tilde{\mathbf{w}}(t+1)$ with given $\{\tilde{\boldsymbol{\lambda}}(t), \tilde{\boldsymbol{\kappa}}(t), \tilde{\boldsymbol{\gamma}}(t)\}$ and $\{\tilde{\mathbf{u}}(t+1), \tilde{\mathbf{v}}(t+1), \tilde{p}(t+1), \mathbf{z}(t+1)\}$ by solving

$$\begin{aligned} \min_{\tilde{\mathbf{w}}} \ & \sum_{m=1}^{M}\left|\tilde{u}_m(t+1) + \frac{\tilde{\lambda}_m(t)}{\rho} - \tilde{\mathbf{w}}^H\mathbf{a}(\theta_m)\right|^2 \\ & + \sum_{s=1}^{S}\left|\tilde{v}_s(t+1) + \frac{\tilde{\kappa}_s(t)}{\rho} - \tilde{\mathbf{w}}^H\mathbf{a}(\bar{\theta}_s)\right|^2 \\ & + \left|\tilde{\mathbf{w}} - \mathbf{z}(t+1) + \frac{\tilde{\boldsymbol{\gamma}}(t)}{\rho}\right|^2 \end{aligned} \quad (66)$$

which can be represented as

$$\min_{\tilde{\mathbf{w}}} \ \tilde{\mathbf{w}}^H\tilde{\mathbf{R}}\tilde{\mathbf{w}} + \tilde{\mathbf{b}}^H\tilde{\mathbf{w}} + \tilde{\mathbf{w}}^H\tilde{\mathbf{b}} \quad (67)$$

where

$$\tilde{\mathbf{R}} = \sum_{m=1}^{M}\mathbf{a}(\theta_m)\mathbf{a}^H(\theta_m) + \sum_{s=1}^{S}\mathbf{a}(\bar{\theta}_s)\mathbf{a}^H(\bar{\theta}_s) + \mathbf{I}_N \quad (68)$$

$$\begin{aligned} \tilde{\mathbf{b}} = & -\sum_{m=1}^{M}\left(\tilde{u}_m(t+1) + \frac{\tilde{\lambda}_m(t)}{\rho}\right)^*\mathbf{a}(\theta_m) \\ & -\sum_{s=1}^{S}\left(\tilde{v}_s(t+1) + \frac{\tilde{\kappa}_s(t)}{\rho}\right)^*\mathbf{a}(\bar{\theta}_s) \\ & -\mathbf{z}(t+1) + \frac{\tilde{\boldsymbol{\gamma}}(t)}{\rho}. \end{aligned} \quad (69)$$

Therefore, the solution to (67) is given by

$$\tilde{\mathbf{w}} = -\tilde{\mathbf{R}}^{-1}\tilde{\mathbf{b}}. \quad (70)$$

Step 3: Update Lagrange multiplier elements or vector as

$$\tilde{\kappa}_s(t+1) = \tilde{\kappa}_s(t) + \rho(\tilde{v}_s(t+1) - \tilde{\mathbf{w}}^H(t+1)\mathbf{a}(\bar{\theta}_s)) \quad (71)$$

$$\tilde{\lambda}_m(t+1) = \tilde{\lambda}_m(t) + \rho(\tilde{u}_m(t+1) - \tilde{\mathbf{w}}^H(t+1)\mathbf{a}(\theta_m)) \quad (72)$$

for $m = 1, \ldots, M$ and $s = 1, \ldots, S$, and

$$\tilde{\boldsymbol{\gamma}}(t+1) = \tilde{\boldsymbol{\gamma}}(t) + \rho(\tilde{\mathbf{w}}(t+1) - \mathbf{z}(t+1)). \quad (73)$$

Steps 1–3 are repeated until a predefined maximum iteration number T or all $\max_m |\tilde{u}_m(t+1) - \tilde{\mathbf{w}}^H(t+1)\mathbf{a}(\theta_m)| \leq 10^{-4}$, $\max_s |\tilde{v}_s(t+1) - \tilde{\mathbf{w}}^H(t+1)\mathbf{a}(\bar{\theta}_s)| \leq 10^{-4}$ and $\max_n |\tilde{w}_n(t+1) - z_n(t+1)| \leq 10^{-4}$ are reached. Finally, according to (43)–(45) we have

$$e^q = \frac{1}{\xi^2} \quad (74)$$

$$\mathbf{w} = \frac{\tilde{\mathbf{w}}}{\xi} \quad (75)$$

$$e^p = \frac{\tilde{p}}{\xi^2}. \quad (76)$$

Based on Steps 1–3, the proposed beampattern synthesis with constant modulus constraint is summarized in Algorithm 2.

Regarding the computational complexity, we consider the major part, namely, multiplications involved in one iteration. In Algorithm 1, Steps 1–3 require $\mathcal{O}(S^2 + M^2)$, $\mathcal{O}(N^3)$, and $\mathcal{O}(SN + MN)$, respectively; whereas Algorithm 2 requires $\mathcal{O}(S^2)$, $\mathcal{O}(N^3)$, and $\mathcal{O}(SN + MN + N)$ for Steps 1–3, respectively.

TABLE I
ANTENNA ELEMENT POSITIONS

Element index	Position (λ)	Element index	Position (λ)	Element index	Position (λ)	Element index	Position (λ)
1	0	9	3.3170	17	6.3406	25	9.6483
2	0.4060	10	3.7353	18	6.7389	26	9.9393
3	0.9013	11	4.1223	19	7.3355	27	10.3631
4	1.1388	12	4.4168	20	7.7003	28	10.7491
5	1.6367	13	4.8704	21	8.0920	29	11.2905
6	2.0607	14	5.2460	22	8.5186	30	11.5522
7	2.4128	15	5.5802	23	8.7627	31	12.0816
8	2.7776	16	5.9990	24	9.1572	32	12.3660

Algorithm 2 Beampattern Synthesis With Constant Modulus Constraint

Initialization: $\{\boldsymbol{\lambda}(0), \boldsymbol{\kappa}(0), \tilde{\boldsymbol{\gamma}}(0), \mathbf{w}(0)\}$, and T;
for $t = 0, \ldots, T$
Obtain $\xi(t+1)$ and $z_n(t+1)\}$ using (53)-(56);
Obtain $\{\tilde{u}_m(t+1)\}$ using (57);
Obtain $\tilde{p}(t+1)$ and $\tilde{v}_s(t+1)$ using (58)-(65);
Determine $\tilde{\mathbf{w}}(t+1)$ using (66)-(70);
Update $\{\tilde{\kappa}_s(t+1), \tilde{\lambda}_m(t+1), \tilde{\gamma}(t+1)\}$ using (71)-(73);
end for $t = T$ or all the $\max_m |\tilde{u}_m(t+1) - \tilde{\mathbf{w}}^H(t+1)\mathbf{a}(\theta_m)| \le 10^{-4}$, $\max_s |\tilde{v}_s(t+1) - \tilde{\mathbf{w}}^H(t+1)\mathbf{a}(\bar{\theta}_s)| \le 10^{-4}$, and $\max_n |\tilde{w}_n(t+1) - z_n(t+1)| \le 10^{-4}$ are satisfied.
Compute $\mathbf{w}_{opt}$ using (75).

V. SIMULATION RESULTS

Simulations are conducted to assess the performance of the proposed methods. According to the problem formulations in (2) and (3), we divide the simulation section into three parts, i.e., the beampattern synthesis without magnitude constraints, constant modulus beampattern synthesis, and phase-only beampattern synthesis.

A. Beampattern Synthesis Without Magnitude Constraints

1) Experiment 1: Beampattern Synthesis for Linear Arrays: In this experiment, we consider the WLLM beampattern synthesis problem without magnitude constraints [i.e., the synthesis problem shown in (2)] for linear arrays, where $\rho = 10$ and $T = 10\,000$ are employed.

First we simulate a 32-element linear array with random locations [in unit of wavelength, generated via the MATLAB code $13 * rand(32, 1)$], as shown in Table I. The mainlobe and sidelobe regions are set as $[-15°, 15°]$ and $[-90°, -26°] \cup [26°, 90°]$, respectively. The angle sampling interval is 1°. For comparison purposes, we implement the semidefinite relaxation (SDR) method [16], [34], which actually solves the relaxed matrix-optimization version of the original vector-optimization beampattern synthesis problem by dropping the rank-1 constraint [34]. In Fig. 1(a), we show the normalized synthesis result with its minimal mainlobe level, that is

$$\frac{|\mathbf{w}^H\mathbf{a}(\theta)|^2}{\min_{\theta_m} |\mathbf{w}^H\mathbf{a}(\theta_m)|^2} \tag{77}$$

for $\theta = -90°, -89°, \ldots, 90°$. In addition, the generated $\max_{\bar{\theta}_s} |\mathbf{w}^H\mathbf{a}(\bar{\theta}_s)|^2$ and $\min_{\theta_m} |\mathbf{w}^H\mathbf{a}(\theta_m)|^2$ by Algorithm 1 are marked in red in Fig. 1(a). For comparison, we also normalize the results with the corresponding maximal mainlobe levels, as shown in Fig. 1(b). From the results, it is seen that Algorithm 1 can attain the lower sidelobe level (−69.057 dB, contrasting to its minimal mainlobe level) than SDR (−60.487 dB, implemented via minimizing the sidelobe level) [16]. However, comparing the maximal mainlobe level, the SDR method attains more lower sidelobe levels at the cost of large ripples in the mainlobe region. Therefore, in some sense, the proposed method can ensure the synthesis performance in the worst case, where the interference appears at the angle with the maximal sidelobe level and the target appears at the angle with the minimal mainlobe level. Besides, Fig. 1(c) and (d) plot the amplitudes (normalized) and phases of the obtained complex excitations, respectively. To test the effect of the number of iterations on the convergence property of Algorithm 1, we compute the errors $\max_m |u_m - \mathbf{w}^H\mathbf{a}(\theta_m)|$ and $\max_s |v_s - \mathbf{w}^H\mathbf{a}(\bar{\theta}_s)|$ between the auxiliary variables and angular responses (AVARs) in all the 10 000 iterations, which are plotted in Fig. 1(e). We see that after 4000 iterations, the AVAR errors are less than $10^{-(96.27/20)}$ (i.e., −96.27 dB), which shows that Algorithm 1 converges within 10 000 iterations. Obviously, the number of iterations $T = 10\,000$ is set reasonably for Algorithm 1.

Then we test the effect of mutual coupling on the proposed methods for linear arrays. As shown in [35]–[38], a banded symmetric Toeplitz matrix can be used as the model for the mutual coupling of uniform linear array (ULA). Therefore, here we consider a 32-element ULA with half-wavelength element spacing. The banded symmetric Toeplitz matrix is produced using $c_1 = 0.3527 + j0.4584$, $c_2 = 0.1618 - j0.2853$, and $c_3 = 0.0927 - j0.1167$ (see [35], [36], [38] for detail). For comparison, we implement Algorithm 1 with and without mutual coupling cases, and plot the synthesis results, and corresponding amplitudes and phases of complex excitations in Fig. 1(f)–(h), from which we can see that the sidelobe levels with and without mutual coupling are −78.86 and −78.99 dB, respectively. The result shows that the mutual coupling has less effect on the proposed method for beampattern synthesis.

2) Experiment 2: Beampattern Synthesis for Planar Arrays: This experiment considers a beampattern synthesis problem without magnitude constraints for a nonuniform rectangular array composed of $N = 11 \times 11$ isotropic antenna elements arranged in the xy plane of the Cartesian system [see Fig. 2(a)]. Unless stated otherwise, for the following 2-D

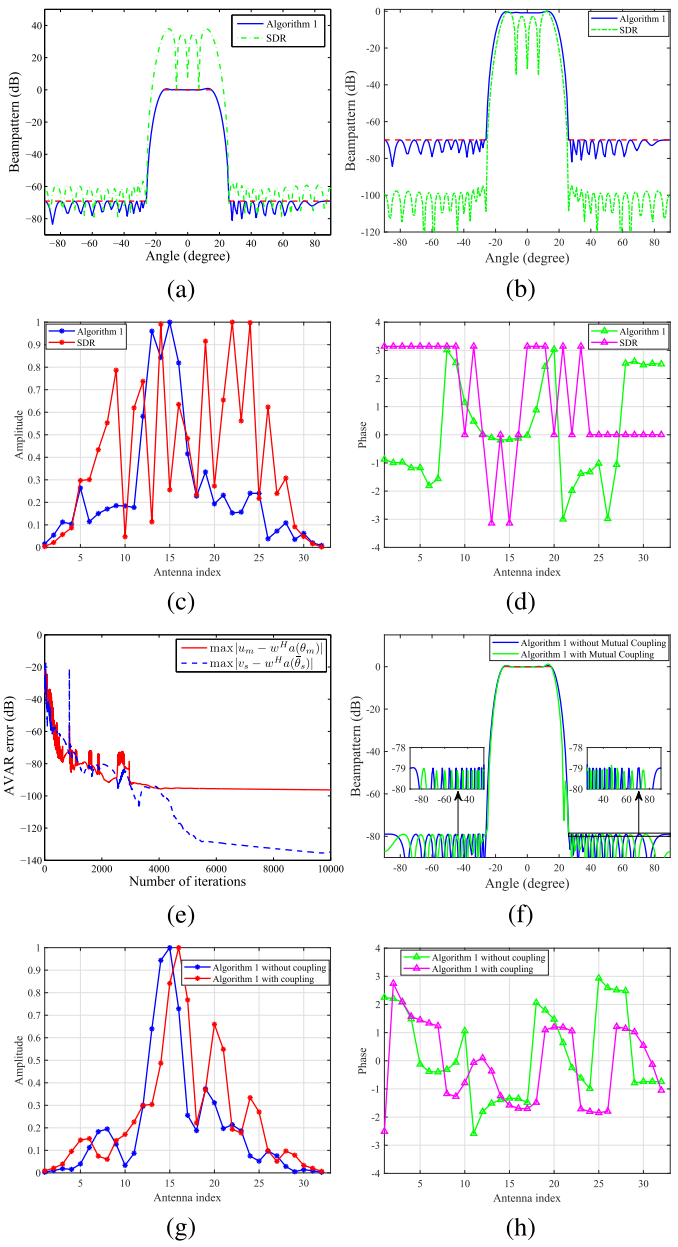

Fig. 1. Simulation results in Experiment 1. (a)–(e) Linear array with arbitrary element positions. (f)–(h) ULA with coupling. (a) Synthesized beampatterns (Normalized with minimal mainlobe level). (b) Synthesized beampatterns (Normalized with maximal mainlobe level). (c) (Normalized) Amplitudes of the excitations of Fig. 1(a) and (b). (d) Phases of the excitations of Fig. 1(a) and (b). (e) AVAR errors versus number of iterations (see Algorithm 1). (f) Synthesized beampatterns with coupling (Normalized with minimal mainlobe level). (g) (Normalized) amplitudes of the excitations of Fig. 1(f). (h) Phases of the excitations of Fig. 1(f).

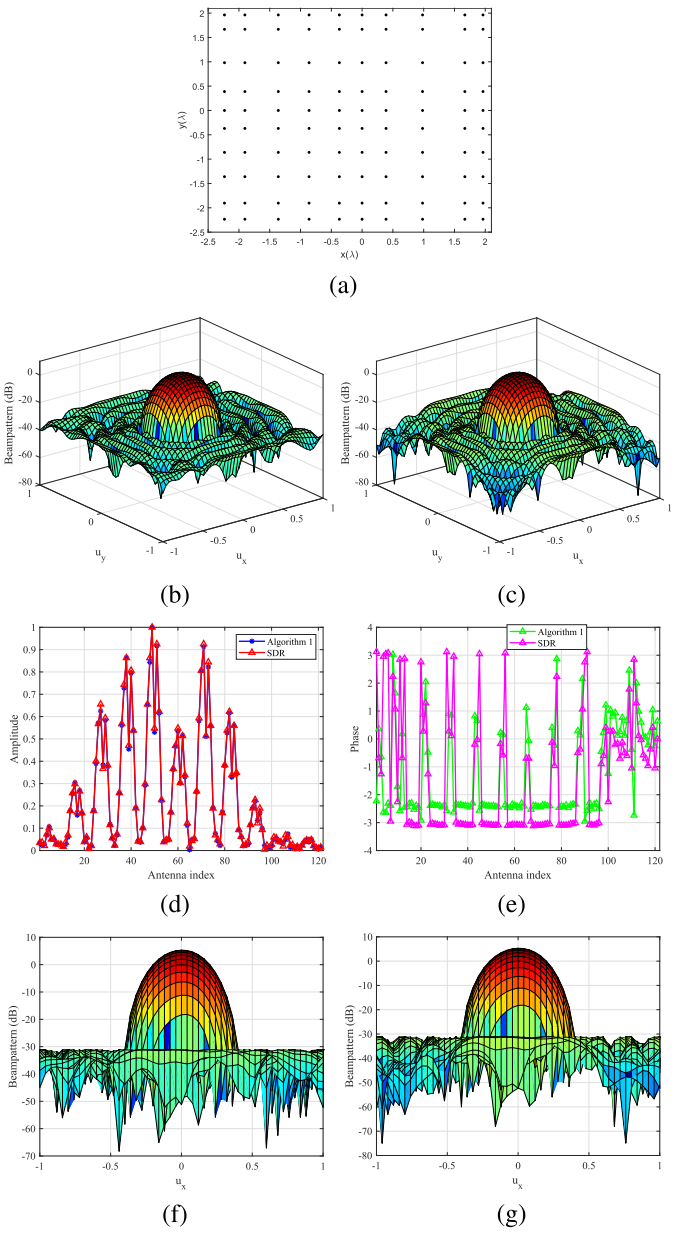

Fig. 2. Simulation results in Experiment 2. (a) Asymmetric rectangular antenna array configuration. (b) 3-D exhibitions of synthesized beampatterns for Algorithm 1. (c) 3-D exhibitions of synthesized beampatterns for SDR. (d) (Normalized) Amplitudes of the excitations of Fig. 2(b) and (c). (e) Phases of the excitations of Fig. 2(b) and (c). (f) 2-D exhibition of Fig. 2(b) for Algorithm 1. (g) 2-D exhibition of Fig. 2(c) for SDR.

planar arrays, all synthesis radiation patterns are plotted in u_x- and u_y-axes, the sampling interval is 0.04 for the u_x- and u_y-directions. The mainlobe region is set as $u_x^2 + u_y^2 \leq 0.2^2$ and sidelobe region is $u_x^2 + u_y^2 \geq 0.4^2$. For the 2-D pattern synthesis problem, we compare our results with the SDR algorithm [34] (implemented via minimizing the sidelobe level). To find out that which beampattern has the lower sidelobe level contrasting to the corresponding minimal mainlobe level, we compute the normalized beampatterns (3-D exhibitions), which are given in Fig. 2(b) and (c), respectively. We also plot corresponding amplitudes and phases in Fig. 2(d) and (e), respectively. Besides, for the sake of readability, we plot 2-D exhibition in the u_x-direction in Fig. 2(f) and (g). It can be seen that the attained sidelobe level by Algorithm 1 is -31.14 dB, which is lower than that of SDR [34] (-31.13 dB). Furthermore, the run times of Algorithm 1 and SDR are 623.78 and 5471.3 s[1], respectively, which indicates the computational efficiency of the former.

[1]All simulation results are implemented on a PC with Intel i7-6700 CPU and RAM 16GB.

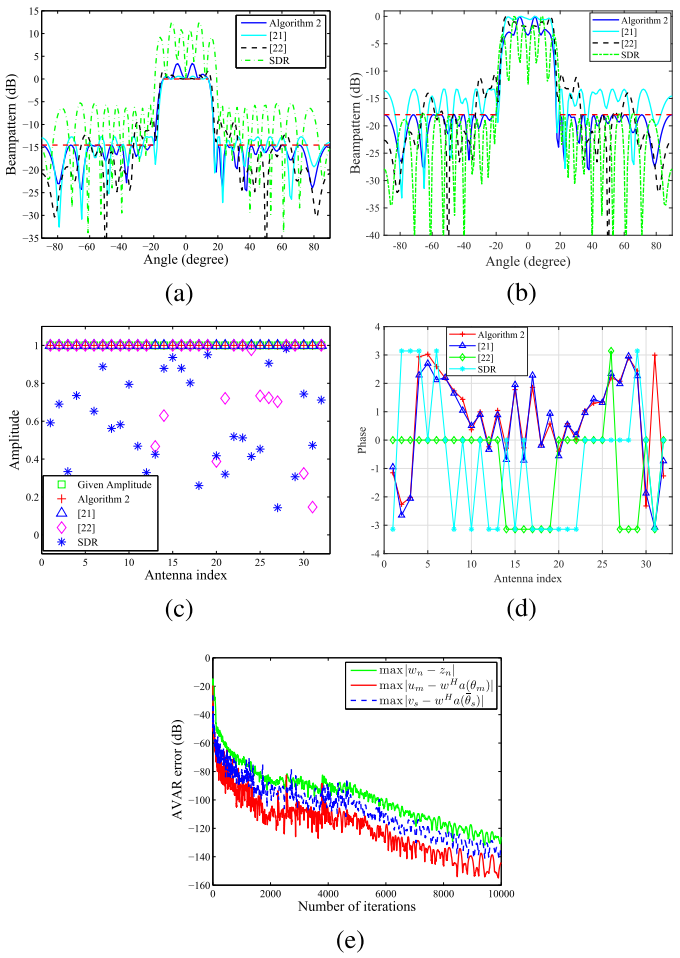

Fig. 3. Simulation results in Experiment 3. (a) Synthesized beampatterns by Algorithm 2, [21], [22], and SDR (Normalized with minimal mainlobe level). (b) Synthesized beampatterns by Algorithm 2, [21], [22], and SDR (Normalized with maximal mainlobe level). (c) Realized magnitudes by Algorithm 2, [21], [22], and SDR. (d) Realized phases by Algorithm 2, [21], [22], and SDR. (e) AVAR errors versus number of iterations (see Algorithm 2).

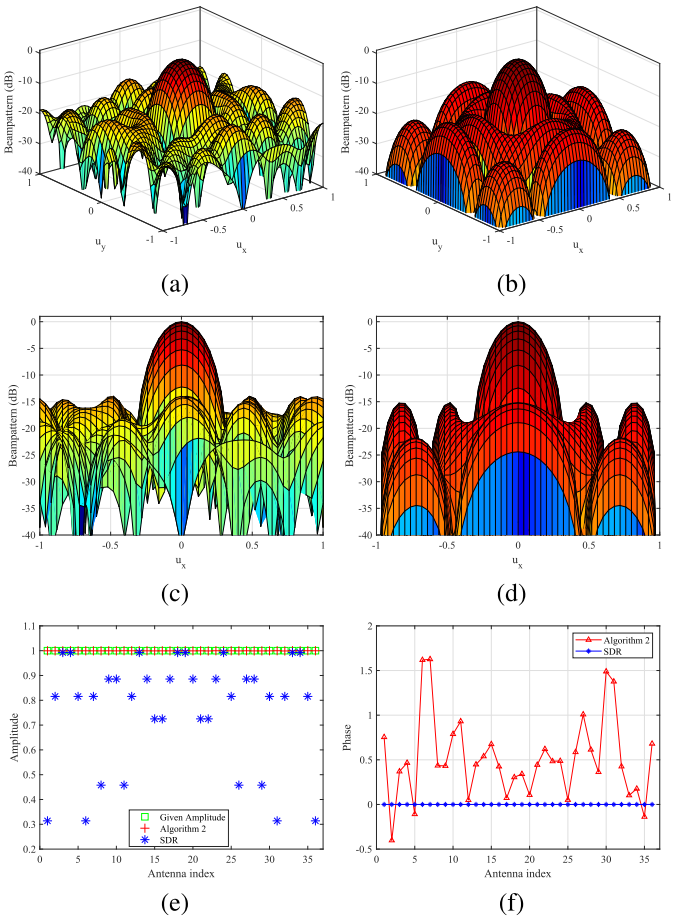

Fig. 4. Simulation results in Experiment 4. (a) 3-D exhibitions of synthesized beampatterns by Algorithm 2. (b) 3-D exhibitions of synthesized beampatterns by SDR. (c) 2-D exhibition of (a) by Algorithm 2. (d) 2-D exhibition of (b) by SDR. (e) Realized magnitudes by Algorithm 2 and SDR. (f) Realized phases by Algorithm 2 and SDR.

B. Constant Modulus Beampattern Synthesis

1) Experiment 3: Constant Modulus Beampattern Synthesis for Linear Arrays: In the third experiment, we consider the WLLM beampattern synthesis problem with constant modulus (e.g., 1) constraints for linear arrays. In this experiment, we use the same nonuniform linear array configuration as that of the first experiment. We set the mainlobe and sidelobe regions as $[-14°, 14°]$ and $[-90°, -20°] \cup [20°, 90°]$, respectively. The methods in [21], [22], and SDR [34] are implemented for comparison purposes. Among them, [21] maximizes the scaling factor to maintain a given pattern shape; whereas the method in [22] relaxes the constant modulus constraint to a convex constraint and then applies alternating optimization to solve the relaxed problem.

As stated in [22], one needs to specify the mask carefully for constant modulus beampattern synthesis problem due to the lost degrees-of-freedom of weight elements in the constant modulus case [21], [22]. However, it must be pointed out that we do not need to specify masks for Algorithm 2. To find out which beampattern has the lowest sidelobe level contrasting to the corresponding minimal mainlobe level and maximal mainlobe level, we compute the normalized beampatterns, respectively, with minimal mainlobe level and maximal mainlobe level and plot the corresponding results in Fig. 3(a) and (b), which further shows that no matter how we adopt the minimal or maximal mainlobe level normalization scheme, the attained sidelobe level by Algorithm 2 is lower than those of [21], [22], and SDR [34] (implemented via minimizing the sidelobe level). Besides, the attained magnitudes and phases are plotted in Fig. 3(c) and (d) to check whether the constant modulus can be realized for all the weight elements by all the methods. We find out that Algorithm 2 and [21] can attain the expected magnitudes, whereas the method in [22] fails. Moreover, we compute the AVAR errors of Algorithm 2 in each iteration and plot them in Fig. 3(e), which shows that the AVAR errors generally decrease with the increase in iterations and are less than -100 dB after 6500 iterations.

2) Experiment 4: Constant Modulus Beampattern Synthesis for Planar Arrays: This experiment considers a constant modulus beampattern synthesis problem with a uniform rectangular array composed of $N = 6 \times 6$ isotropic antenna elements with interelement spacing $\lambda/2$. The mainlobe region is set

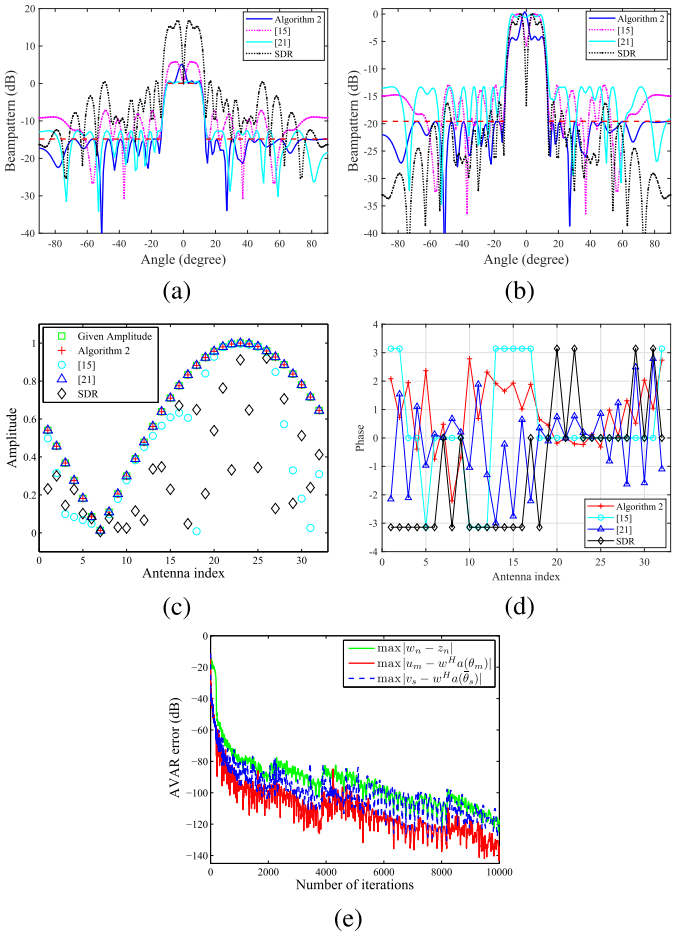

Fig. 5. Simulation results in Experiment 5. (a) Synthesized beampatterns by Algorithm 2, [15], [21], and SDR (Normalized with minimal mainlobe level). (b) Synthesized beampatterns by Algorithm 2, [15], [21], and SDR (Normalized with maximal mainlobe level). (c) Realized magnitudes by Algorithm 2, [15], [21], and SDR. (d) Realized phases by Algorithm 2, [15], [21], and SDR. (e) AVAR error versus number of iterations (see Algorithm 2).

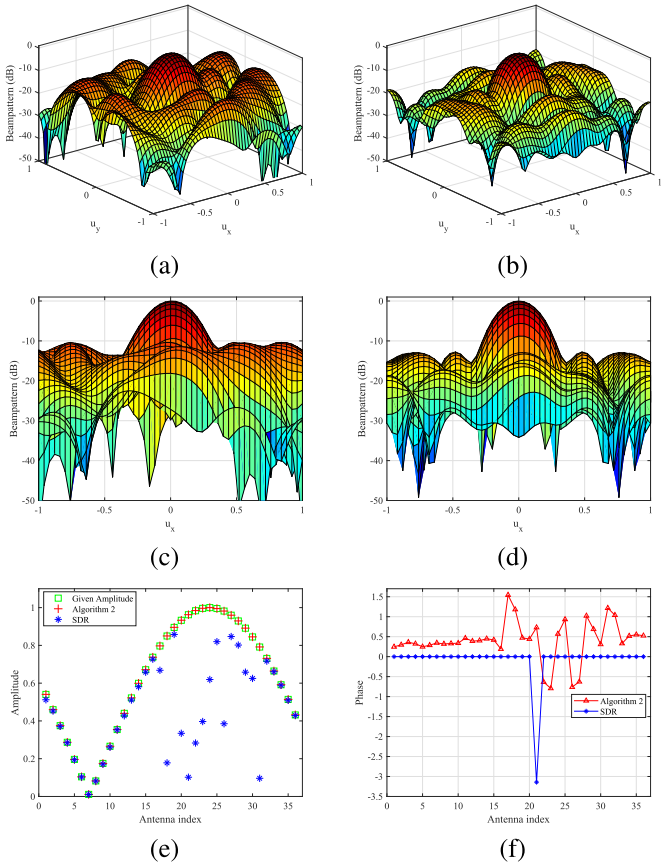

Fig. 6. Simulation results in Experiment 6. (a) 3-D exhibitions of synthesized beampatterns by Algorithm 2. (b) 3-D exhibitions of synthesized beampatterns by SDR. (c) 2-D exhibition of (a) by Algorithm 2. (d) 2-D exhibition of (b) by SDR. (e) Realized magnitudes by Algorithm 2 and SDR. (f) Realized phases by Algorithm 2 and SDR.

as $u_x^2 + u_y^2 \leq 0.02^2$ and sidelobe region is $u_x^2 + u_y^2 \geq 0.3^2$. Initial point is set as $\mathbf{w} = 0.01e^{j(n-0.5N)^2\pi/150}, n = 0, \ldots, N-1$. Similar to Experiment 2, we compare our results with the SDR algorithm [34] (implemented via minimizing the sidelobe level). We plot the 3-D exhibitions of the beampattern synthesis results (normalized with minimal mainlobe level) by Algorithm 2 and SDR in Fig. 4(a) and (b), respectively, and their 2-D exhibitions in the u_x-direction are given in Fig. 4(c) and (d), respectively. We find out that the attained sidelobe level by Algorithm 2 is -13.99 dB, which is higher than that of SDR [34], which are -15.21 dB. However, it can be seen from Fig. 4(e) and (f), reporting the realized amplitudes and phases by Algorithm 2 and SDR, that Algorithm 2 can attain the expected magnitudes, whereas the SDR method fails in ensuring that all the obtained weight elements have constant modulus. Therefore, as far as the constant modulus beampattern synthesis is concerned, the SDR method cannot achieve the task.

C. Phase-Only Beampattern Synthesis

1) Experiment 5: Phase-Only Beampattern Synthesis for Linear Arrays: In the fifth experiment, we consider the WLLM beampattern synthesis with given weight magnitudes. In this experiment, we set the mainlobe and sidelobe regions as $[-10°, 10°]$ and $[-90°, -14°] \cup [14°, 90°]$, respectively. As stated in [15] and [39], slow-varying magnitudes are often adopted to avoid large amplitude hop and simplify the feeding network design from the engineering realization viewpoint. Therefore, we simulate similar sinusoid-type magnitudes as those of [15] and [39], marked in green in Fig. 5(c). The methods in [15], [21], and SDR [34] are implemented for comparison purposes. Similar to Experiments 1 and 3, the normalized beampatterns with minimal and maximal mainlobe levels are plotted in Fig. 5(a) and (b). Besides, the attained magnitudes and phases by all the methods are given in Fig. 5(c) and (d), respectively. Moreover, the AVAR errors obtained by Algorithm 2 are plotted in Fig. 5(e). From the results, we can see that: 1) the results display the characteristics of the proposed method in attaining sufficiently lower sidelobe levels no matter how either minimal or maximal mainlobe level is applied for normalization; 2) Algorithm 2 and [21] can attain the prescribed magnitudes, whereas both the algorithm in [15] and SDR method fail in ensuring that all the obtained weight elements have the prescribed magnitudes; and 3) Algorithm 2 exhibits the well convergence property.

2) Experiment 6: Phase-Only Beampattern Synthesis for Planar Arrays: The same configuration is adoped as that of Experiment 4 apart from the given magnitudes shown in green in Fig. 6(e). The mainlobe region is set as $u_x^2 + u_y^2 \leq 0.02^2$ and sidelobe region is $u_x^2 + u_y^2 \geq 0.3^2$. Initial point is set as $\mathbf{w} = 0.1e^{j(n-0.7N)^2\pi/150}, n = 0, \ldots, N-1$, and $\rho = 14$. Similar to Exps. 2 and 4, we compare our results with the SDR algorithm [34] (implemented via minimizing the sidelobe level). We plot the 3-D exhibition of beampattern synthesis results (normalized with minimal mainlobe level) and their 2-D u_x-direction exhibitions in Fig. 6(a)–(d). Furthermore, the realized amplitudes and phases by Algorithm 2 and SDR are reported in Fig. 6(e)–(f), which shows that the SDR method fails in realizing the prescribed magnitudes, whereas Algorithm 2 can guarantee that all the obtained weight elements have expected modulus. It can be observed from Fig. 6(a)–(d) that the attained sidelobe level by Algorithm 2 is -10.38 dB, which is higher than that of SDR [34], -12.64 dB. However, we must point out that the SDR method fails in ensuring that all the obtained weight elements have the prescribed magnitudes, as shown in Fig. 6(e).

From the six experiments, we see that: 1) the formulated models in (2) and (3), i.e., minimizing the ratio of the maximal sidelobe level to the minimal mainlobe level, can help us to attain sufficiently low sidelobe level with respect to the minimal mainlobe level; 2) the proposed algorithms are developed from ADMM, and thus inherited its superior convergence property [24]; and 3) the proposed methods can avoid specifying a possibly improper or infeasible pattern mask.

VI. Conclusion

In this article, we devise a novel approach to array beampattern synthesis without specifying lobe level masks. Via minimizing the ratio of the maximal sidelobe level to the minimal mainlobe level, we attain low sidelobe level relative to the mainlobe level. To solve the resultant fractional program, we develop an ADMM-based method and also extend it to the phase-only and constant modulus pattern synthesis problems.

Appendix A: Phase-only Pattern

For the phase-only beampattern synthesis problem [16]–[20], the magnitudes of weight elements are specified, i.e., $|\omega_n| = M_n$ for $n = 1, \ldots, N$.

Note that ω_n can be rewritten as $\omega_n = M_n \nu_n$, where ν_n is of unit modulus, i.e., $|\nu_n| = 1$. Thus, we represent $\mathbf{w}$ as $\mathbf{w} = \Gamma \boldsymbol{\nu}$, where $\Gamma = \text{diag}\{M_1, \ldots, M_N\}$ and $\boldsymbol{\nu} = [\nu_1, \ldots, \nu_N]^T$.

Obviously the elements of the vector $\boldsymbol{\nu}$ are of the constant modulus now. Therefore, the pattern $|\mathbf{w}^H \mathbf{a}(\bar{\theta}_s)|^2$ and $|\mathbf{w}^H \mathbf{a}(\theta_m)|^2$ become $|\mathbf{w}^H \mathbf{a}(\bar{\theta}_s)|^2 = |\boldsymbol{\nu}^H \Gamma \mathbf{a}(\bar{\theta}_s)|^2$ and $|\mathbf{w}^H \mathbf{a}(\theta_m)|^2 = |\boldsymbol{\nu}^H \Gamma \mathbf{a}(\theta_m)|^2$, respectively. Now the phase-only beampattern synthesis problem is represented as standard constant modulus one

$$\begin{aligned} \min_{\boldsymbol{\nu}} \quad & \frac{\max_{\bar{\theta}_s} |\boldsymbol{\nu}^H \hat{\mathbf{a}}(\bar{\theta}_s)|^2}{\min_{\theta_m} |\boldsymbol{\nu}^H \hat{\mathbf{a}}(\theta_m)|^2} \\ \text{s.t.} \quad & |\nu_n| = 1, \quad n = 1, \ldots, N \end{aligned} \tag{78}$$

where $\hat{\mathbf{a}}(\bar{\theta}_s) = \Gamma \mathbf{a}(\bar{\theta}_s)$ and $\hat{\mathbf{a}}(\theta_m) = \Gamma \mathbf{a}(\theta_m)$.

Obviously, the phase-only synthesis problem of $\mathbf{w}$ in [15] and [16] is transformed into a constant modulus synthesis problem of $\boldsymbol{\nu}$ [21], [22], as shown in (78).

Appendix B: ADMM

ADMM is applicable to problems which can be formulated as the following constrained optimization:

$$\begin{aligned} \min_{\mathbf{x},\mathbf{z}} \quad & f(\mathbf{x}) + g(\mathbf{z}) \\ \text{s.t.} \quad & \mathbf{A}\mathbf{x} + \mathbf{B}\mathbf{z} = \mathbf{c}. \end{aligned} \tag{79}$$

The augmented Lagrangian constructed from (79) is then

$$\mathcal{L}(\mathbf{x}, \mathbf{z}, \boldsymbol{\lambda}) = f(\mathbf{x}) + g(\mathbf{z}) + \boldsymbol{\lambda}^T (\mathbf{A}\mathbf{x} + \mathbf{B}\mathbf{z} - \mathbf{c}) + \frac{\rho}{2} \|\mathbf{A}\mathbf{x} + \mathbf{B}\mathbf{z} - \mathbf{c}\|^2 \tag{80}$$

where $\rho > 0$ and $\boldsymbol{\lambda}$ are the step size and Lagrange multiplier vector, respectively. The ADMM solves (80) via the decomposition–coordinated procedure and the resultant iterative updating steps are

$$\mathbf{x}(t+1) = \arg\min_{\mathbf{x}} \ \mathcal{L}(\mathbf{x}, \mathbf{z}(t), \boldsymbol{\lambda}(t)) \tag{81}$$

$$\mathbf{z}(t+1) = \arg\min_{\mathbf{z}} \ \mathcal{L}(\mathbf{x}(t+1), \mathbf{z}, \boldsymbol{\lambda}(t)) \tag{82}$$

$$\boldsymbol{\lambda}(t+1) = \boldsymbol{\lambda}(t) + \rho(\mathbf{A}\mathbf{x}(t+1) + \mathbf{B}\mathbf{z}(t+1) - \mathbf{c}) \tag{83}$$

where t denotes the iteration number. The interested reader is referred to [24] for detail.

Appendix C: Algorithm Extension

We discuss the extension of the proposed algorithms to other radiation patterns, including narrow beam pattern, and notch pattern.

On the one hand, when the main region $\{\theta_1, \ldots, \theta_M\}$ reduces into a single angle point, e.g., $\{\theta_1\}$, $\min_{\theta_1} |\mathbf{w}^H \mathbf{a}(\theta_1)|^2 = |\mathbf{w}^H \mathbf{a}(\theta_1)|^2$, and Algorithms 1 and 2 are also applicable to the narrow beam pattern synthesis problem.

On the other hand, in some practical applications, except for the main region $\{\theta_1, \ldots, \theta_M\}$ and sidelobe region $\{\bar{\theta}_1, \ldots, \bar{\theta}_S\}$, we expect to attain L notches at the L angles $\{\tilde{\theta}_1, \ldots, \tilde{\theta}_L\}$. Let η_l denote the anticipated ratio of the sidelobe level to the lth notch level, that is

$$\frac{\max_{\bar{\theta}_s} |\mathbf{w}^H \mathbf{a}(\bar{\theta}_s)|^2}{|\mathbf{w}^H \mathbf{a}(\tilde{\theta}_l)|^2} \geq \eta_l \tag{84}$$

for $l = 1, \ldots, L$, and define

$$\bar{\mathbf{a}}(\bar{\theta}_s) = \begin{cases} \mathbf{a}(\bar{\theta}_s), & s = 1, \ldots, S \\ \sqrt{\eta_{s-S}}\mathbf{a}(\tilde{\theta}_{s-S}), & s = S+1, \ldots, S+L. \end{cases} \tag{85}$$

Then we replace the term $\max_{\bar{\theta}_s} |\mathbf{w}^H \mathbf{a}(\bar{\theta}_s)|^2$ in (2) and (3) with $\max_{\bar{\theta}_s} |\mathbf{w}^H \bar{\mathbf{a}}(\bar{\theta}_s)|^2$ and thus Algorithms 1 and 2 are also suitable for the notch pattern synthesis problem.

REFERENCES

[1] F. Wang, V. Balakrishnan, P. Zhou, J. Chen, R. Yang, and C. Frank, "Optimal array pattern synthesis using semidefinite programming," *IEEE Trans. Signal Process.*, vol. 51, no. 5, pp. 1172–1183, May 2003.

[2] H. Lebret and S. Boyd, "Antenna array pattern synthesis via convex optimization," *IEEE Trans. Signal Process.*, vol. 45, no. 3, pp. 526–532, Mar. 1997.

[3] Z. Shi and Z. Feng, "A new array pattern synthesis algorithm using the two-step least-squares method," *IEEE Signal Process. Lett.*, vol. 12, no. 3, pp. 250–253, Mar. 2005.

[4] S. E. Nai, W. Ser, Z. L. Yu, and H. Chen, "Beampattern synthesis for linear and planar arrays with antenna selection by convex optimization," *IEEE Trans. Antennas Propag.*, vol. 58, no. 12, pp. 3923–3930, Dec. 2010.

[5] B. Fuchs, "Synthesis of sparse arrays with focused or shaped beampattern via sequential convex optimizations," *IEEE Trans. Antennas Propag.*, vol. 60, no. 7, pp. 3499–3503, Jul. 2012.

[6] D. G. Leeper, "Isophoric arrays-massively thinned phased arrays with well-controlled sidelobes," *IEEE Trans. Antennas Propag.*, vol. 47, no. 12, pp. 1825–1835, Dec. 1999.

[7] S. Holm, B. Elgetun, and G. Dahl, "Properties of the beampattern of weight- and layout-optimized sparse arrays," *IEEE Trans. Ultrason., Ferroelectr., Freq. Control*, vol. 44, no. 5, pp. 983–991, Sep. 1997.

[8] O. M. Bucci, M. D'urso, T. Isernia, P. Angeletti, and G. Toso, "Deterministic synthesis of uniform amplitude sparse arrays via new density taper techniques," *IEEE Trans. Antennas Propag.*, vol. 58, no. 6, pp. 1949–1958, Jun. 2010.

[9] Y. Liu, Q. Huo Liu, and Z. Nie, "Reducing the number of elements in the synthesis of shaped-beam patterns by the forward-backward matrix pencil method," *IEEE Trans. Antennas Propag.*, vol. 58, no. 2, pp. 604–608, Feb. 2010.

[10] O. Quevedo-Teruel and E. Rajo-Iglesias, "Ant colony optimization in thinned array synthesis with minimum sidelobe level," *IEEE Antennas Wireless Propag. Lett.*, vol. 5, pp. 349–352, 2006.

[11] A. Trucco, E. Omodei, and P. Repetto, "Synthesis of sparse planar arrays," *Electron. Lett.*, vol. 33, no. 22, pp. 1834–1835, Oct. 1997.

[12] S. Nai, W. Ser, Z. Yu, and S. Rahardja, "A robust adaptive beamforming framework with beampattern shaping constraints," *IEEE Trans. Antennas Propag.*, vol. 57, no. 7, pp. 2198–2203, Jul. 2009.

[13] O. M. Bucci, G. Franceschetti, G. Mazzarella, and G. Panariello, "Intersection approach to array pattern synthesis," *IEE Proc. H—Microwaves, Antennas Propag.*, vol. 137, no. 6, pp. 349–357, 1990.

[14] G. Poulton, "Antenna power pattern synthesis using method of successive projections," *Electron. Lett.*, vol. 22, no. 20, pp. 1042–1043, 1986.

[15] B. Fuchs, "Application of convex relaxation to array synthesis problems," *IEEE Trans. Antennas Propag.*, vol. 62, no. 2, pp. 634–640, Feb. 2014.

[16] P. J. Kajenski, "Phase only antenna pattern notching via a semidefinite programming relaxation," *IEEE Trans. Antennas Propag.*, vol. 60, no. 5, pp. 2562–2565, May 2012.

[17] P. J. Kajenski, "Phase-only monopulse pattern notching via semidefinite programming," in *Proc. IEEE Int. Symp. Antennas Propag.* Chicago, IL, USA: APS, Jul. 2012, pp. 1–2.

[18] R. Shore, "Nulling a symmetric pattern location with phase-only weight control," *IEEE Trans. Antennas Propag.*, vol. AP-32, no. 5, pp. 530–533, May 1984.

[19] O. Bucci, G. Mazzarella, and G. Panariello, "Reconfigurable arrays by phase-only control," *IEEE Trans. Antennas Propag.*, vol. 39, no. 7, pp. 919–925, Jul. 1991.

[20] R. Vescovo, "Reconfigurability and beam scanning with phase-only control for antenna arrays," *IEEE Trans. Antennas Propag.*, vol. 56, no. 6, pp. 1555–1565, Jun. 2008.

[21] J. Liang, X. Fan, W. Fan, D. Zhou, and J. Li, "Phase-only pattern synthesis for linear antenna arrays," *IEEE Antennas Wireless Propag. Lett.*, vol. 16, pp. 3232–3235, 2017.

[22] P. Cao, J. S. Thompson, and H. Haas, "Constant modulus shaped beam synthesis via convex relaxation," *IEEE Antennas Wireless Propag. Lett.*, vol. 16, pp. 617–620, 2017.

[23] J. Liang, X. Zhang, H. C. So, and D. Zhou, "Sparse array beampattern synthesis via alternating direction method of multipliers," *IEEE Trans. Antennas Propag.*, vol. 66, no. 5, pp. 2333–2345, May 2018.

[24] S. Boyd, N. Parikh, E. Chu, B. Peleato, and J. Eckstein, "Distributed optimization and statistical learning via the alternating direction method of multipliers," *Found. Trends Mach. Learn.*, vol. 3, no. 1, pp. 1–122, 2011.

[25] D. Gabay, "Applications of the method of multipliers to variational inequalities," in *Augmented Lagrangian Methods: Applications to the Solution of Boundary-Value Problems*. Amsterdam, The Netherlands: North-Holland, 1983.

[26] J. Eckstein and D. P. Bertsekas, "On the Douglas–Rachford splitting method and the proximal point algorithm for maximal monotone operators," *Math. Program.*, vol. 55, nos. 1–3, pp. 293–318, Apr. 1992.

[27] M. Hong, Z.-Q. Luo, and M. Razaviyayn, "Convergence analysis of alternating direction method of multipliers for a family of nonconvex problems," *SIAM J. Optim.*, vol. 26, no. 1, pp. 337–364, Jan. 2016.

[28] J. Liang, H. C. So, J. Li, and A. Farina, "Unimodular sequence design based on alternating direction method of multipliers," *IEEE Trans. Signal Process.*, vol. 64, no. 20, pp. 5367–5381, Oct. 2016.

[29] T. Erseghe, "A distributed and maximum-likelihood sensor network localization algorithm based upon a nonconvex problem formulation," *IEEE Trans. Signal Inf. Process. Netw.*, vol. 1, no. 4, pp. 247–258, Dec. 2015.

[30] W. Fan, J. Liang, and J. Li, "Constant modulus MIMO radar waveform design with minimum peak sidelobe transmit beampattern," *IEEE Trans. Signal Process.*, vol. 66, no. 16, pp. 4207–4222, Aug. 2018.

[31] J. Liang, H. So, J. Li, A. Farina, and D. Zhou, "On optimizations with magnitude constraints on frequency or angular responses," *Signal Process.*, vol. 145, pp. 214–224, Apr. 2018.

[32] S. Boyd and L. Vandenberghe, *Convex Optimization*. Cambridge, U.K.: Cambridge Univ. Press, 2004.

[33] D. P. Bertsekas, *Constrained Optimization and Lagrange Multiplier Methods*. New York, NY, USA: Academic, 1982.

[34] Z.-Q. Luo, W.-K. Ma, A. So, Y. Ye, and S. Zhang, "Semidefinite relaxation of quadratic optimization problems," *IEEE Signal Process. Mag.*, vol. 27, no. 3, pp. 20–34, May 2010.

[35] T. Svantesson, "Modeling and estimation of mutual coupling in a uniform linear array of dipoles," in *Proc. Int. Conf. Acoust., Speech Signal Process.*, Phoenix, AZ, USA, vol. 5, Mar. 1999, pp. 2961–2964.

[36] T. Svantesson, "Mutual coupling compensation using subspace fitting," in *Proc. IEEE Sensor Array Multichannel Signal Process. Workshop*, Waltham, MA, USA, vol. 1, Mar. 2000, pp. 494–498.

[37] J. Liang, X. Zeng, W. Wang, and H. Chen, "L-shaped array-based elevation and azimuth direction finding in the presence of mutual coupling," *Signal Process.*, vol. 91, no. 5, pp. 1319–1328, May 2011.

[38] Z. Ye and C. Liu, "On the resiliency of MUSIC direction finding against antenna sensor coupling," *IEEE Trans. Antennas Propag.*, vol. 56, no. 2, pp. 371–380, Feb. 2008.

[39] J. Wang, Y. Zheng, and Z. He, *Optimization of Array Antenna Synthesis, in Antenna Array Theory and Engineering Application*, B. Jing, Ed., 1st ed. Beijing, China: Publishing House of Electronics Industry (in Chinese), 2015, pp. 228–234.

Junli Liang was born in China. He received the Ph.D. degree from the Chinese Academy of Sciences, Beijing, China, in 2007.

He is currently working as a Professor with the School of Electronics and Information, Northwestern Polytechnical University, Xi'an, China. His research interests include radar signal processing, array signal processing, and image processing and their applications.

Xuhui Fan was born in China. She is currently pursuing the Ph.D. degree with the School of Electronics and Information, Northwestern Polytechnical University, Xi'an, China.

Her research interest includes array signal processing and its applications.

Hing Cheung So (Fellow, IEEE) was born in Hong Kong. He received the B.Eng. degree from the City University of Hong Kong, Hong Kong, and the Ph.D. degree from The Chinese University of Hong Kong, Hong Kong, in 1990 and 1995, respectively, all in electronic engineering.

From 1990 to 1991, he was an Electronic Engineer with the Research and Development Division, Everex Systems Engineering Ltd., Hong Kong. From 1995 to 1996, he was a Post-Doctoral Fellow with The Chinese University of Hong Kong. From 1996 to 1999, he was a Research Assistant Professor with the Department of Electronic Engineering, City University of Hong Kong, where he is currently a Professor. His research interests include detection and estimation, fast and adaptive algorithms, multidimensional harmonic retrieval, robust signal processing, source localization, and sparse approximation.

Dr. So is an Elected Member of the Signal Processing Theory and Methods Technical Committee, IEEE Signal Processing Society, from 2011 to 2016, where he is the Chair of the awards subcommittee from 2015 to 2016. He was on the Editorial Boards of the *IEEE Signal Processing Magazine* from 2014 to 2017, the IEEE TRANSACTIONS ON SIGNAL PROCESSING from 2010 to 2014, *Signal Processing* in 2010, and *Digital Signal Processing* in 2011. He is also the Lead Guest Editor of the IEEE JOURNAL OF SELECTED TOPICS IN SIGNAL PROCESSING—Special Issue on Advances in Time/Frequency Modulated Array Signal Processing in 2017.

Deyun Zhou was born in China. He received the Ph.D. degree from Northwestern Polytechnical University, Xi'an, China, in 1991.

He is currently working as a Professor with the School of Electronics and Information, Northwestern Polytechnical University. His research interests include control engineering and applications.